MOLECULAR DESIGN OF POLYMERS FOR LASER STRUCTURING AND THIN OXIDE FILMS BY PULSED LASER DEPOSITION AS MODEL SYSTEM FOR ELECTROCHEMICAL APPLICATIONS

THOMAS LIPPERT
Paul Scherrer Institut, General Energy Research Department, 5232 Villigen PSI, Switzerland; E-mail: thomas.lippert@psi.ch

Abstract. This work reviews the interaction of photons with polymers with an emphasis on UV laser ablation. Polymethylmethacrylate, polyimides and special designed polymers are used as examples to show that the mechanism is a mixture of photochemical and photothermal features which are closely related to the polymer structure and properties. Different approaches to probe the ablation mechanisms and to improve ablation are discussed. A critical evaluation of the experimental procedures and analysis techniques is presented. In the second part the pulsed laser deposition of thin oxides films is considered. Perovskite films and Li-spinel films are analyzed in great details and used as examples of two model systems that are appropriate for application in re-chargeable batteries.

Keywords: Laser ablation, designed polymers, PLD, PRCLA, perovskite, Lithium Spinel, thin film

1. Introduction

1.1. ABLATION OF POLYMERS

The interactions of photons with a polymer can result in a large variety of reactions which range from the modification of the polymer surface to the complete decomposition. The latter usually results in the ablation and/or carbonization of the irradiated polymer area. The first reports about laser ablation of polymers were published in 1982[1,2] and since then numerous studies dealing with ablation of a wide variety of polymers and the ablation mechanism(s) have been published and are well summarized in various

J.J. Dubowski and S. Tanev (eds.), Photon-based Nanoscience and Nanobiotechnology, 267–306.

higher pressures of background gases are other important factors. PLD has been successfully used for the growth of many types of multicomponent thin films with a very high quality.[6,23] Nevertheless, some limitations exist, such as particulates, incongruent ablation and oxygen deficiency in oxide materials. To minimize these limitations some modifications to the traditional PLD method have been developed. Some examples for these modifications are Aurora-PLD,[24] RF plasma assisted pulsed laser deposition,[25,26] PLD with an electric field applied to the substrate,[27] UV assisted PLD,[28] off-axis PLD,[29] magnetic-field PLD,[30] and pulsed reactive crossed-beam laser ablation (PRCLA).[31]

The first report on the combination of a pulsed gas supply with PLD was published by Gupta and Hussey in 1991.[32] This setup allows the application of low background pressures, which enables the implementation of *in-situ* vacuum characterization techniques, e.g. reflection high-energy electron diffraction (RHEED). The main difference between this setup and the PRCLA setup used in our studies (Fig. 1) is the distance of the gas pulse to the ablation spot on the target.

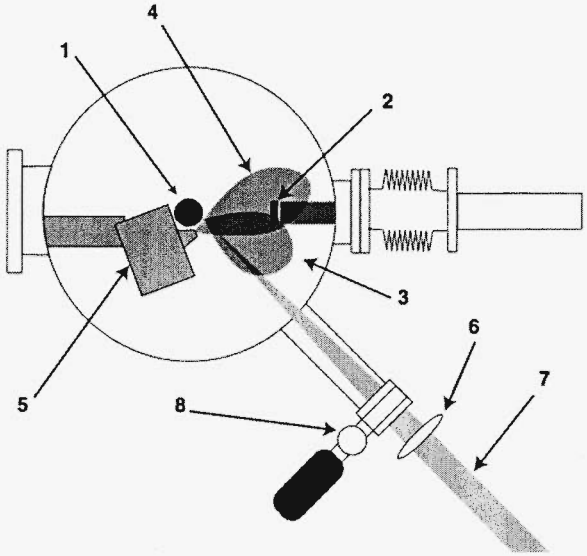

Figure 1. Pulsed reactive cross-beam laser deposition setup: 1) cylindrical target rod, 2), heated and rotating substrate 3) expanding plasma plume generated by the laser, 4) expanding pulsed gas, 5) nozzle of the gas pulse generator, 6) focusing lens, 7) laser beam, 8) inlet for oxygen.

For PRCLA the distance is smaller than 10 mm, which allows an increase of the gas phase interaction and the probability of reactive scattering between the gas pulse and plasma, while the resulting species

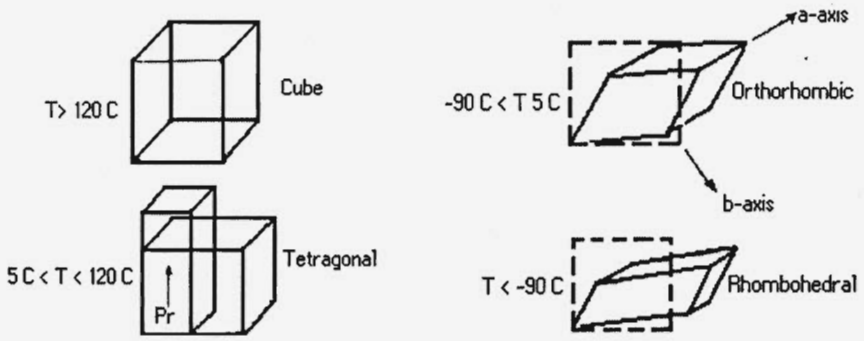

Figure 2. Different perovskite structures.

The perovskite structure possesses a very high degree of compositional flexibility, which allows to accommodate a wide variety of A and B cations, and is also tolerant for large concentrations of both oxygen and cation vacancies. In some complex composition the A and B sites can be occupied by more than one cation species ($A_{1-x}A'_xB_{1-y}B'_yO_3$). In the case of the B sites this can involve cations of more than one element (chemical variation), or different oxidation states of the same element (charge variation).

The physical properties of the perovskite-type materials, such as ferroelectric, dielectric, pyroelectric, and piezoelectric behaviour, will depend on the cation ordering, anion vacancies, and changes in the structural dimensionality. The ongoing research does not only cover the study of magnetic and electronic properties,[41] but also the development of new materials to optimize renewable energy sources, i.e. solid oxide fuel cells[42], direct methanol fuel cells, and metal/air batteries.[43]

The most important topic for the production of metal/air batteries (i.e. Zn/air) is the development of new materials for anodes and cathodes. These materials have to be stable under long term operation conditions (acidic or alkaline medium with an applied potential), and should be cheaper than the commonly used noble metal materials, i.e. Pt. The Zn/air battery is the battery that offers one of the highest storage densities, which is due to the fact that one of the components in the reaction comes from outside of the battery, i.e. atmospheric oxygen from the air as cathode reactant. The recent design of a re-chargeable Zn air battery consists of two electrodes, i.e. Zn paste and a bifunctional oxygen electrode with an integrated electrocatalyst for reduction and evolution of oxygen.[44,45] However, one major problem associated with the development of these secondary batteries is the limited lifetime of the bifunctional electrode (which catalyzes the reduction and the evolution of oxygen). The development of a stable catalyst is still a

Co). The 8*a* tetrahedral and 16*c* octahedral sites of the Mn_2O_4 framework form a diamond type network. The empty sites are interconnected by common faces and edges to form a three-dimensional pathway for the lithium diffusion (see Fig. 3, right). The angles formed by the consecutive straight spokes, 8*a* - 16*c* - 8*a* measure about 107°. In the case of $LiMn_2O_4$, the lattice constant of the unit cell is 8.247 Å. However, in inverse spinels, where a part of the transition metal ions situated in the 16*d* sites displace the lithium ions in the 8*a* sites and prevent easier diffusion of lithium ions from 8*a* to other 8*a* sites via vacant octahedral 16*c* sites. The lithium intercalation has long been demonstrated for LiM_2O_4 (with M= Ti, V, Mn) with a capacity of one additional lithium atom per formula unit at room temperature.[50-55] In addition to that, some studies were carried out on more complex spinel type phases such as $Li_2Mn_4O_9$, $Li_4Mn_5O_{12}$, $Li_4Ti_5O_{12}$, $LiFe_5O_8$, etc.[56-59]

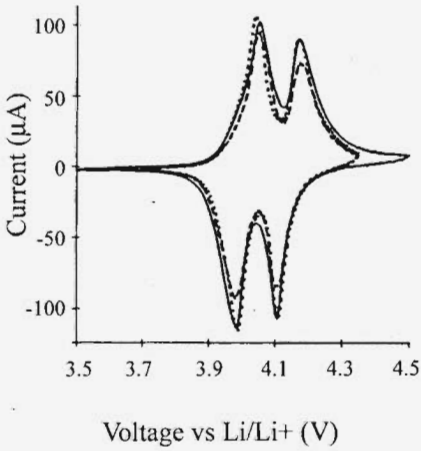

Figure 4. Cyclic voltammogram of three 0.3 μm thick $LiMn_2O_4$ in 1M $LiPF_6$/EC/DMC (1:2), 1 mV/s. Aadopted from [61].

During charge and discharge of the battery, the lithium ions are extracted and reintercalated respectively into the spinel framework. In Fig. 4 a typical cyclic voltammogram in the 3.4 to 4.5 V range of a $LiMn_2O_4$ film produced by PLD onto stainless steel substrates is shown. The four peaks correspond to the intercalation/deintercalation of the Li-ions into the spinel phase. The first step is usually located between 3.9 and 4.1 V (in this case at 4.03 V). It corresponds to the extraction of lithium from half of the tetrahedral sites during charging. The second peak is situated between at 4.17 V and corresponds to the extraction from the rest of the Li ions. The Li-Li interaction forces are much stronger after extraction of the first part of

wavelength. The final step of the PMMA decomposition is the unzipping of the polymer, to yield the monomer. It is noteworthy to mention, that one chain end radical will yield around 6 monomers at room temperature and over 200 at temperatures above the glass transition temperature (T_g = 104 °C). This unzipping reaction is also observed for other polymers such as Teflon and polystyrene. The small fragments, i.e. CH_4, CO, and CH_3OH, the detection of the monomer, and of the double bonds (chain end or in-chain) upon incubation and laser ablation are again clear indications for the involvement of photochemical reactions in the laser ablation process of PMMA. One other important fact is the difference of the products for UV and IR laser irradiation of PMMA. The monomer is the exclusive product upon irradiation with a CO_2 laser,[65] which is a clear indication for a pure thermal process, i.e. heating of the polymer above the ceiling temperature, while UV irradiation yields a rather broad mixture of products. The pronounced differences of the ablation products between UV and mid-IR irradiation and the clear signs for photochemical reaction in PMMA suggest strongly that the clear division of the ablation mechanism into photothermal or photochemical is at least questionable for UV laser ablation.

2.1.2. *Laser Ablation of Selected Polymers*

In an attempt to study the ablation mechanism of PMMA and to apply longer irradiation wavelengths, i.e. 308 nm, which may be economically more interesting, various dopants to induce absorption at this wavelength have been tested. These dopants range from polyaromatic compounds, such as pyrene, to compounds which contain a photochemical active group.[66] The utilization of dopants allows also to decouple the absorption site, i.e. the dopant, from the polymer main chain. The polyaromatic compounds reveal a photothermal mechanism which has been modeled by a cyclic multiphoton absorption mechanism where the triplet states play a key role.[67] The photochemical active compounds have been selected to test whether the properties of the dopants have a pronounced influence on the ablation properties. For these studies various dopants, based on the triazene group (-N=N-N<), have been tested, which are photochemically well studied[68-70] and which release also a large amount of nitrogen during the photochemical decomposition. It has also been suggested that the nitrogen or other released gases may act a driving force of ablation, which carries larger ablation fragments away from the surface. A detailed study of the ablation properties of PMMA doped with these triazene compounds revealed that very high ablation rates of up to 80 μm per pulse could be reached at high laser fluences and low doping levels, i.e. 0.5 to 1 wt.-%. A weak relation between the photochemical activity, i.e. the quantum yield, and the ablation rates was suggested.[71] A clear sign for the release of the gaseous products,

α_{lin}, reaching almost 200 000 cm^{-1}. Typical absorption spectra of a triazene and a polyimide polymer are shown in Figure 6.

The spectrum reveals also one of the very interesting properties of the triazene polymers, i.e. the two absorption maxima that can be clearly assigned to the aromatic system (around 200 nm) and the triazene unit (around 330 nm).[72] This allows to selectively excite various chromophores of the polymer by switching from 193 to 248 and 308 nm irradiation.

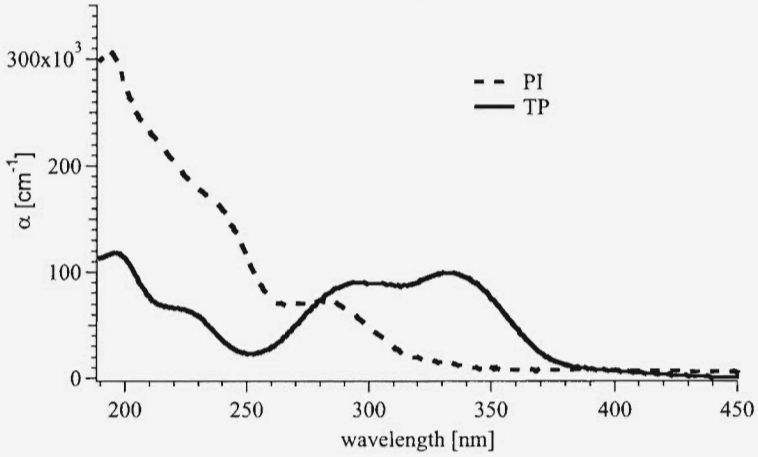

Figure 6. UV-Vis absorption spectra of thin films of a triazene polymer (structure shown in Figure 7) and of a soluble polyimide (similar in structure to Kapton™).

2.1.3. *Ablation of Polyimides and Triazene Polymers*

The detailed comparison of the ablation rates of a polyimide, PI (i.e. Kapton™ HN), and the triazene polymer (with the chemical structure shown in Figure 7) is shown in Figure 8 for irradiation at 308 nm where both polymers exhibit almost the same linear absorption coefficients. The data were analyzed from multi-pulse experiments using the slope of etch depths versus pulse number plots.

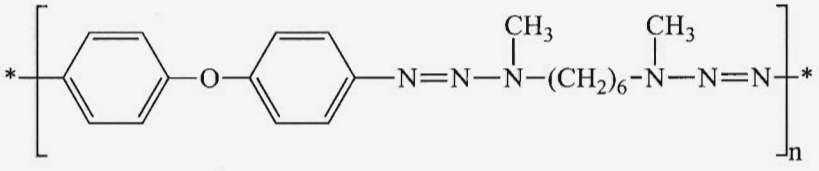

Figure 7. Chemical structure of the triazene polymer which has been used for the UV-Vis absorption spectra and most ablation experiments.

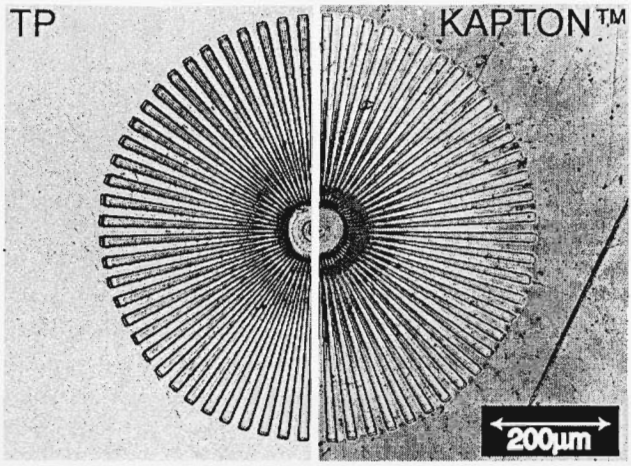

Figure 9. Ablation pattern in TP1 (left) and Kapton™ (right) created by 308 nm irradiation using a gray tone phase mask.

The structure in TP is much sharper and the re-deposited carbon material that is clearly visible for PI is absent. This modification of the surface has been studied for both materials using various analytical tools, such as X-ray photoelectron spectroscopy (XPS) and confocal Raman microscopy.[76, 77] In the case of TP no chemical and physical surface modification was detected for ablation at 308 nm with fluences above the threshold of ablation. The change of the surface composition of Kapton™ has been analyzed in detail by XPS[78] and confocal Raman microscopy.[79] The data show clearly that the ablation structures are surrounded by a carbon layer which is depending on the applied fluence and number of pulses, while inside the structures carbonization was also detected, but with a slightly higher degree of crystallinity for the carbon.[78]

It is noteworthy to mention in this context that "polyimide" (PI) is probably the most studied polymer in laser ablation. Polyimide is also the material for which most ablation models are applied, but great care has to be taken for which polyimide the data are obtained. Polyimide is not single polymer, but describes a class of polymers which contain at least one cyclic imide group (shown in Figure 11) per repetition unit. Even Kapton™ is not one polymer, but there are also many different types of Kapton™, which are defined with additional letters, e.g. HN.

In the context of comparing ablation data it is also very important to be very careful, as the usual ablation parameter, such as ablation rate, d(f), threshold fluence, F_0, and effective absorption coefficient, α_{eff}, are strongly influenced by the method that was applied for determining these values.

method of measuring the ablation depth. This can be done my "mechanical" methods with a tip, e.g. profilometry or atomic force microscopy, where changes of the surface morphology are detected. Another method is a gravimetric method, i.e. quartz crystal microbalance (QMB), where the weight loss is measured. The latter can and will also detect reactions inside the polymer layer which are associated with a weight loss, e.g. loss of N_2 for the triazene polymer, but not with the creation of an ablation crater that is measured by the "mechanical" methods.

2.1.4. *Ablation Mechanisms*

Various approaches to obtain a better understanding of the ablation mechanisms were developed and may be divided into three different methods:

- Changing the polymer structure
- Time-resolved measurements during ablation and
- Varying the laser pulse lengths and wavelengths.

Various polymers have been designed to study the influence of the chemical structure on the ablation behavior.[85-88] The tested polymers included the triazene-polymers, polymers based on photoactive ester groups, and mixed polymers that contained both groups (ester and triazene). The polymers were compared considering the threshold fluence and ablation rate at low fluences. The lowest thresholds and highest ablation rates were found for the triazene group containing polymers. The linear absorption coefficients are within the tested range (10 000 to 100 000 cm^{-1}) only of minor importance. It is also noteworthy to mention that the triazene polymer with the highest density of the photochemical active triazene groups per repetition unit (TP) reveals the highest ablation rates. The order of the ablation rates also follows quite well the order of photochemical decomposition in solution using low fluences and low concentrations of the polymer in solution (in the range of 10^{-5} Mol l^{-1}).[85] Excimer lamps were also employed to study the effect of low fluence irradiation at 222 and 308 nm, where linear (no ablation) photochemistry is expected.[89] Excimer lamps emit incoherent, quasi-continuous radiation at the same wavelength as the excimer laser. At the low photon fluxes provided by the lamps, multi-photon processes can be neglected. Decomposition of the triazene chromophore was detected by UV-spectroscopy for 222 and 308 nm irradiation, while decomposition of the aromatic chromophore was detected only at 222 nm. This is consistent with the absence of surface carbonization for 308 nm irradiation and the detection of carbonization for 248 nm

contrast, corresponding images of polyimide for 351 nm irradiation reveal pronounced swelling, followed by material removal that persists for microseconds after the laser pulse.[100,101]

Significantly, surface reflectivity measurements (probed at 532 nm) during ablation at 308 nm show a decrease in reflectivity (darkening) during the laser pulse (included in Figure 10) which recovers completely after the laser pulse.[97]

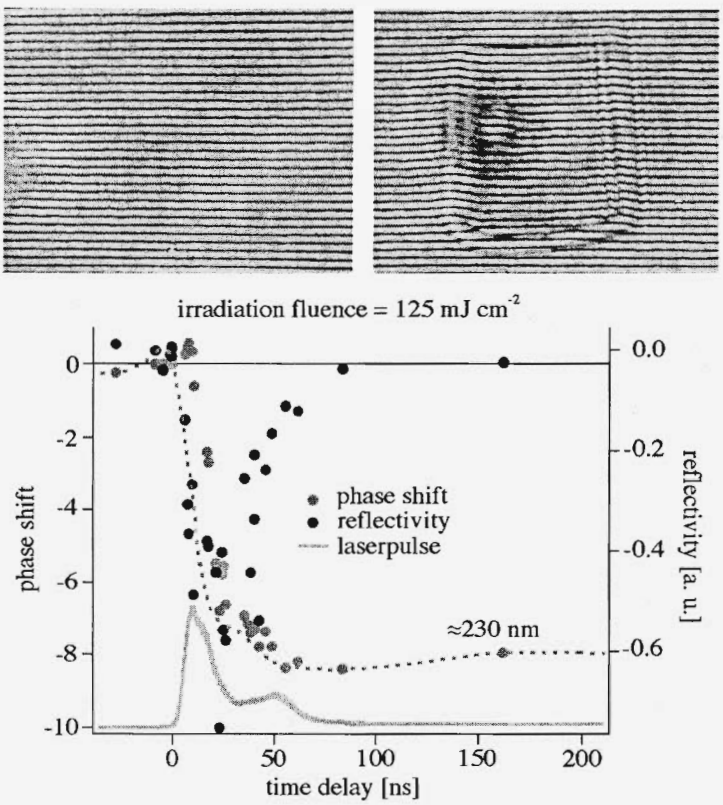

Figure 10. Surface interferometric analysis of the ablation process for TP1 and an irradiation wavelength of 308 nm. Top left: Interference image prior to irradiation; top right: interference image after a delay time of 160 ns. Bottom: analysis of a complete set of interferometric images using a FFT routine which yields the phase shift (depth) and reflectivity.

Insight into the ablation mechanisms is also provided by studying of the ablation products, e.g. by mass-spectrometry. It is noteworthy to mention that time-resolved mass spectrometry at 248 and 308 nm irradiation identified all the expected fragments of the decomposition of TP1 (shown

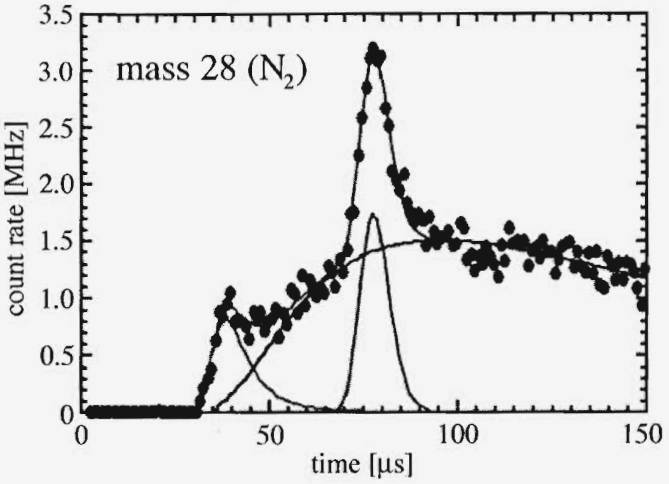

Figure 12. Time of flight curve for mass 28 obtained for 308 nm irradiation of the TP.

Ablation of polymers will therefore always be a mixture between photochemical and photothermal reactions, where the ratio between these two is influenced by the material, i.e. mainly thermal for polymers such as Teflon and with more pronounced photochemical features for photoactive polymers. The photochemical features are, e.g. the bleaching of the triazene chromophore during the pulse, the ablation starting and ending with the laser pulse, and the very fast or metastable ablation products.

2.2. PULSED LASER DEPOSITION OF THIN OXIDE FILMS

2.2.1. *Parameter which Influence Thin Film Growth of Perovskites*

When PLD is performed under vacuum conditions, two main aspects are different from sputtering or conventional thermal evaporation techniques. First, pulses of high vapour fluxes (~ 1 ms) are separated by periods of no vapour flux (~ 100 ms) and relatively high vapour arrival energies at the substrate. Second, there are ions with energies in the keV range and neutral atoms with energies of several eV. PLD can also be performed in the presence of a background gas, e.g. oxygen, two effects are expected during the film formation: the reduction of the kinetic energy of the vapour flux, and a high flux of background oxygen molecules bombarding the surface during deposition. This high flux could change the film and substrate surface energies and will increase the oxygen content (for oxide films). The first arriving pulse causes the nucleation of a high density of smaller

conditions. The film thickness measured by a profilometer is around 500 nm (after 42000 pulses) with a roughness in the range of 4-5 nm for 21 000 pulses. The composition of the films, measured by RBS, is $La_{0.64\pm0.05}Ca_{0.35\pm0.05}Co_{0.95\pm0.05}O_{3\pm0.05}$, suggesting an almost perfectly congruent material transfer.

The effect of different oxygen sources during PRCLA on the oxygen content of the grown films was studied by applying only the oxygen background (8×10^{-4} mbar), or only the gas pulse (N_2O at 2 bar) or both together, during the deposition process. The compositions of the deposited films are presented in Table 2.

Table 2. Stoichiometry of the LCCO films produced with different oxygen sources.

Film	Deposition Condition	Stoichiometry
A	Gas pulse (2 bar)	$La_{0.68\pm0.05}Ca_{0.32\pm0.05}Co_{0.93\pm0.05}O_{2.6\pm0.05}$
B	Oxygen background (8×10^{-4} mbar)	$La_{0.6\pm0.05}Ca_{0.4\pm0.05}Co_{0.98\pm0.05}O_{2.75\pm0.05}$
C	Gas pulse (2 bar) + oxygen back.	$La_{0.68\pm0.05}Ca_{0.32\pm0.05}Co_{0.91\pm0.05}O_{2.91\pm0.05}$

The composition of the films changes with the different deposition conditions. When the films are grown in the presence of 8×10^{-4} mbar of oxygen background, lower amounts of La and Ca are observed, while the best oxygen stoichiometry is obtained when the films are deposited using the gas pulse and the oxygen background. The presence of only one oxidizing source always produces films with lower oxygen content. The effect of different gases during the formation of multicomponent metal-oxides has been investigated for a long time.[32,108] The oxygen requirements during the growth of oxides are controlled by the oxidation kinetics and the thermodynamic phase stability at the growth temperature.[32] When PLD is used as the film growing technique, a large amount of material is deposited in a very short time separated by periods with no vapor flux. This makes it necessary to have a high flux of oxygen available to oxidize the species that arrive at the substrate. In principle, the oxygen could originate exclusively from the oxide target, without the necessity of an additional oxidizing source. However, only a fraction of the oxygen is released as atoms (neutrals and ions), wile the remaining part is ejected as O_2[109]. The adsorption probability of O_2 is less than unity due to the inefficient adsorption at the surface[110] compared to the high sticking probability of atomic O. The fact that the oxygen molecules have a lower probability of remaining at the substrate surface makes it necessary to utilize an additional oxidizing source for the effective oxidation of the cations during the film growth. The flux of oxygen molecules is much lower in the case of the

for PLD)[114]. After the interaction zone the particles propagate freely in the direction of the substrate with almost no collisions with the oxygen molecules of the background gas (8×10^{-4} mbar). The analysis of time and space resolved emission spectra reveal several pronounced differences of PRCLA compared to PLD. First, lower kinetic energies are observed for the species arriving at the substrate. Second, a larger amount of excited states species and (excited) ionic species arrive at the substrate. It is of course important, that the film composition will not change, if the other deposition parameters are varied to optimize/analyze the film growth. A distance between substrate-target of 4.5 cm and a substrate temperature of 650 °C were chosen because epitaxial films could be obtained for these conditions. The results reveal that varying deposition parameters, (i.e. temperature and distance) do not affect the composition of the films, suggesting that the deposition condition can be varied over a wide range without changing the chemical composition of the films. These results can be explained by the fact that the kinetic energy of the ablated species arriving at the substrate (0.74 to 1.99 eV), is too small to cause re-sputtering (typically observed for kinetic energies of »10 eV) of the elements from the growing film.[115] No changes in the stoichiometry are also observed when the distance is kept constant (4.5 cm) and the temperature is varied from 550 °C to 700 °C. This suggests that there is no pronounced re-evaporation of the elements from the growing films at these temperatures.

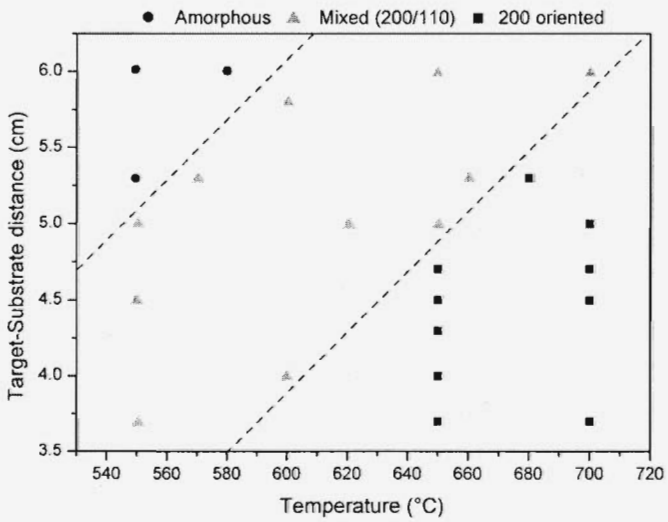

Figure 13. Structure type of LCCO thin film deposited under various conditions of target – to - substrate distance and substrate temperature.

electrodes. In the gas diffusion electrode the surface is porous and the real area of the electrode is extremely difficult to determine. Additionally, the reactive area consists of carbon and catalyst. Contrary to this, the thin film electrode consists of a compact structure with very few small pores. The surface area can be assumed to have a similar value as the geometrical area and only the catalyst is present on the surface. These differences suggest that different adsorption mechanisms are present on both surfaces. If we consider the electron transfer as well, the situation becomes even more complicated due to the fact that for thin films the electron transfer will be possible only through electron holes or oxygen vacancies and determination of their presence in the crystal lattice during the redox-reaction is nearly impossible. For the gas diffusion electrode the electron transfer will take place on different surfaces, i.e. on the perovskite (oxygen evolution) and on the carbon followed by the perovskite (oxygen reduction). Any attempt at a quantitative comparison between the systems will therefore be associated with a large systematic error. Polarization curves reveal that the model systems present a slightly smaller overpotential for the two oxygen reactions than the optimized gas diffusion electrode. The model system is more active for the oxygen evolution reaction while the gas diffusion electrode is more active for the oxygen reduction reaction. An important factor is that current density values are comparable to the ones obtained for the carbon-based perovskite gas diffusion electrodes, indicating that thin films can be used as model system to screen different perovskite electrodes.

2.2.5. *Effect of the Crystallinity on the Electrochemical Activity*

Most of the reported electrochemistry with solid electrodes involves polycrystalline materials. Such electrodes consist of a variety of small domains with different crystal faces and edges which will face the electrolyte. Different crystal faces exhibit different properties (e.g. work function) so that the behavior observed at a polycrystalline electrode represents an average of that for a number of different crystal planes and sites. One possible way to analyze solid electrode interfaces and their influence in a specific reaction can be performed by using single-crystal electrodes. The most common metals used as electrodes, i.e. Pt, Pd, Ag, Ni and Cu, form face-centered cubic crystal structures. Three low index faces (100), (110), and (111) are the surfaces most frequently used as electrodes, because they tend to be stable and can be polished to yield fairly smooth, uniform surfaces. Nevertheless, even the most carefully prepared surfaces are not atomically smooth over areas larger than a few square micrometers, and they inevitably show steps, edges, and defect sites. Catalytic and adsorptive properties of solid surfaces can depend upon the crystal face. An

electrodes, i.e. the adsorption of the oxygen molecules, is affected by the surface energy of the electrode surface, which depends on the exposed crystallographic orientation and grain boundaries. It can also be concluded that the phase with (100) orientation presents the best performance.

2.2.6. *Parameters Influencing the Deposition of Lithium Spinel Films*

In the case of Li-spinels different substrate materials can result in different preferred crystallographic orientation of the deposited film. Several authors[117, 118] have shown that the deposited films form a polycrystalline spinel with random orientation on substrates such as platinum, stainless steel and silicon. However, Rougier et al. have shown that the utilization of $Si(100)/Si_3N_4$ substrates yields to a preferred (111) orientation.[119] Another parameter that influences the crystallinity of the films is the substrate temperature.[120-122] At higher substrate temperatures the characteristic reflexes in the X-ray-diffraction patterns ((111) at 19.5° and (444) at ~ 45°,[122]) increases. These reflexes are associated with the degree of crystallinity of the films. This influence has previously been shown by various authors.[117,120,123,124] who also analyzed the influence of the oxygen background pressure and target composition. Julien et al.[120] revealed that films grown from a target with an excess of 5% of lithium shows very poor crystallinity. With an increasing excess of lithium in the target (up to 15%), the deposited films reach the regular spinel crystal structure, which can also be improved with increasing substrate temperatures. These experiments where carried out at relatively low substrate temperatures, ranging from 100 °C to 300 °C and at a very low background pressure of $6.7x10^{-5}$ mbar of O_2 and with non stoichiometric targets. The necessary experimental parameters may vary from theses values when using a stoichiometric target. As described earlier for the perovskite-type phases, Pulsed Reactive Cross-Beam Laser Deposition (PRCLA) is in principle a very suitable method for the deposition of complex oxides. However, in the case of spinels the utilization of the PRCLA set up is not applicable due to the crossed gas pulse, which significantly increases the scattering of light atoms, such as lithium. Only a minor amount of Li-spinel can be detected in the XRD spectra.

In Fig. 15 the X-ray diffraction (XRD) patterns of $LiMn_2O_4$ deposited on polished titanium using the classical PLD setup (without the gas pulse) at an oxygen pressure of 0.2 mbar and a substrate temperature of 510 °C is shown. A KrF excimer laser (248 nm) with a repetition rate of 10 Hz, a fluence of 3-4 J/cm^2 and 18000 pulses was used for the deposition. The diffraction patterns show clearly the reflexes that can be attributed to a spinel structure of the film which is in agreement with results reported by other groups[117,119,125].

In the first cycle an oxidation peak is observed around 3.6 V. However, this is most probably not related to the extraction of lithium from the lithium manganate spinel but is due to the titanium substrate. The peaks around 3.6 V in the negative current region and the increase of the current at 3.6 V in the positive current region correspond quite well with the peaks found for an uncoated Ti-foil sample (see Fig. 17). The extraction/insertion of lithium from the lithium spinel can be detected as very weak peaks in the voltammogram (see arrows in Fig. 16). These peaks occur in the expected region, i.e. two oxidation peaks between 4.05 V and 4.2 V in the positive current region and two reduction peaks between 3.9 V and 4.1 V in the negative current region. This leads to the conclusion that a spinel phase is present on the substrate. The difference between the first and the following cycles is most probably due to the expected formation of an solid electrolyte interphase (SEI) and, possibly, structural transformation. The pronounced noises in Fig. 16, e.g. between 3.4 and 3.5 V, are currents from the electrochemical reactions of the electrolyte in solution in contact with the non-coated surface of the titanium substrate.

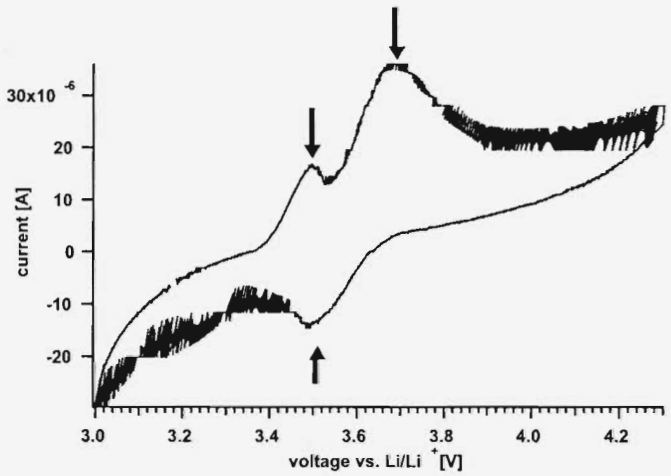

Figure 17. CV of an uncoated titanium foil sample. Arrows mark the extraction and reintercalation of lithium into the titanium-oxide layer.

The RBS/ERDA measurements reveal a strong lithium deficiency (Li/Mn ration between 0.4 and 0.5) for all films deposited under an oxygen background pressure between 0.1 and 0.3 mbar. Nevertheless, the X-ray diffraction patterns in Fig. 15 give clear evidence for the presence of a spinel phase but which may not be homogeneously distributed over the whole substrate. There are two possible ways to overcome this problem. One possibility is to utilize an excess of lithium in the target,[119,120,124] or to optimize the conditions for the classical PLD setup (without the gas pulse).

measurements revealed a spinel phase on all substrates deposited at these conditions, however, electrochemical activity in the expected voltage range was only obtained for films deposited at a background pressure of 0.2 mbar and at a distance between the target and the substrate of 3-4 cm (see Fig. 16). Furthermore, RBS/ERDA measurements revealed a strong deficiency in lithium and oxygen in these films. Whereas the oxygen content can be easily increased by cooling down the sample in pure oxygen atmosphere after deposition, the increase of the lithium content is much more difficult. Characterization of the laser-created plasma with a Langmuir Probe and Mass spectroscopy suggest the presence of high energetic ions (over 50 eV), mainly lithium and manganese, which can resputter the growing film from the substrate. An increase of the background pressure from $1 \cdot 10^{-4}$ mbar to 1 mbar strongly reduces the kinetic energy of these ions, especially of manganese which results in a lower sputtering yield of the ionic species in the plasma. The reduced sputtering yield can be observed by measuring the deposition rate with a Quartz Crystal Microbalance (QCM) for various laser energies and variable background pressures (see Fig. 19). Higher laser fluences result as expected from larger ablation rates in higher growth rates per pulse.

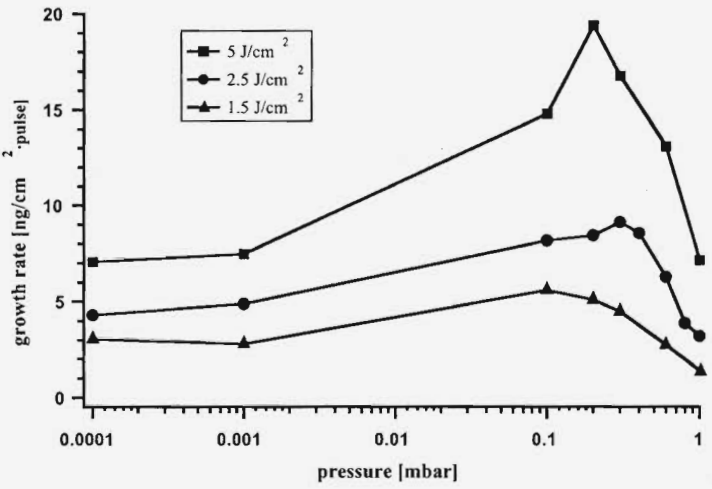

Figure 19. Pressure dependence of the growth rate at constant laser fluence of 1.5, 2.5 and 5 J/cm^2.

The deposition rate first increases with increasing background pressure, then decreases again after reaching a peak around 0.1-0.3 mbar. The position of this peak corresponds to the small window of 0.1 to 0.3 mbar for optimum deposition conditions. It might therefore be possible that the

For the Li-spinels, it can be concluded that the deposition of $LiMn_2O_4$ is most practicable with a standard PLD equipment, but physical constraints such as atom scattering and vapor pressure leave only a small window for the optimum experimental parameters. The optimum conditions are a background pressure around 0.2 mbar and a substrate temperature of 500 °C. However, the lithium deficiency in the deposited film is still an issue. This deficiency is most probably due to the evaporation of lithium from the film and to the sputtering effect of high energetic ions in the plasma at low background pressures. At higher background pressures, these ions are sufficiently slowed down to minimize the damage produced at the film surface. The deposition of stoichiometric $LiMn_2O_4$ from a stoichiometric target has been demonstrated by Morcrette et al.[117,123]. Nevertheless, the utilization of an excess of lithium in the target seems to be the easiest way to compensate for the loss of lithium during deposition. The extraction/insertion of lithium from the lithium spinel could be detected for the films deposited at the optimized conditions. Differences between the first and the following cycles can be assigned most probably to the expected formation of a solid electrolyte interphase (SEI) and, possibly, structural transformation. This proves that thin films are also in the case of Li-ion batteries very good model system to study the fundamental processes of Li intercalation and de-intercalation and of the corresponding interphase processes.

Acknowledgements

This work has been partially supported by the Swiss National Science Foundation.

References

1. R. Srinivasan and V. Mayne-Banton, Self-Developing Photoetching Of Poly(Ethylene-Terephthalate) Films By Far Ultraviolet Excimer Laser-Radiation, *Appl. Phys. Lett.* 41(6), 576-578 (1982).
2. Y. Kawamura, K. Toyoda and S. Namba, Effective Deep Ultraviolet Photoetching Of Poly(Methyl Methacrylate) By An Excimer Laser, *Appl. Phys. Lett.* 40(5), 374-375 (1982).
3. R. Srinivasan and B. Braren, Ultraviolet-Laser Ablation Of Organic Polymers, *Chem. Rev.* 89(6), 1303-1316 (1989).
4. P. E. Dyer, *Photochemical processing of materials*, (Academic Press, London, 1992).
5. S. Lazare and V. Granier, Ultraviolet-Laser Photoablation Of Polymers - A Review And Recent Results, *Laser Chem.* 10(1), 25-40 (1989).
6. D. Bäuerle, *Laser Processing and Chemistry*, (Springer Verlag, Berlin, 2000).

26. C. Vivien, M. Dinescu, P. Meheust, C. Boulmer-Leborgne, A. P. Caricato and J. Perriere, Nitride-molecule synthesis in plasma produced by reactive laser ablation assisted by RF discharge for thin-film deposition, *Appl. Surf. Sci.* 129, 668-673 (1998).
27. A. Narazaki, T. Sato, Y. Kawaguchi, H. Niino, A. Yabe, T. Sasaki and N. Koshizaki, Pulsed laser deposition of semiconductor-ITO composite films on electric-field-applied substrates, *Appl. Surf. Sci.* 197, 438-441 (2002).
28. V. Craciun, D. Craciun, Z. Chen, J. Hwang and R. K. Singh, Room temperature growth of indium tin oxide thin films by ultraviolet-assisted pulsed laser deposition, *Appl. Surf. Sci.* 168(1-4), 118-122 (2000).
29. J. W. Yoon, T. Sasaki and N. Koshizaki, Pressure-controlled preparation of nanocrystalline complex oxides using pulsed-laser ablation at room temperature, *Appl. Phys. A-Mater. Sci. Process.* 76(4), 641-643 (2003).
30. G. Radhakrishnan and P. M. Adams, Pulsed-laser deposition of particulate-free TiC coatings for tribological applications, *Appl. Phys. A-Mater. Sci. Process.* 69, S33-S38 (1999).
31. M. J. Montenegro, M. Dobeli, T. Lippert, S. Muller, B. Schnyder, A. Weidenkaff, P. R. Willmott and A. Wokaun, Pulsed laser deposition of $La_{0.6}Ca_{0.4}CoO_3$ (LCCO) films. A promising metal-oxide catalyst for air based batteries, *Phys. Chem. Chem. Phys.* 4(12), 2799-2805 (2002).
32. A. Gupta and B. W. Hussey, Laser Deposition Of $YBa_2Cu_3O_7$-Delta Films Using A Pulsed Oxygen Source, *Appl. Phys. Lett.* 58(11), 1211-1213 (1991).
33. P. R. Willmott and F. Antoni, Growth of GaN(0001) thin films on Si(001) by pulsed reactive crossed-beam laser ablation using liquid Ga and N_2, *Appl. Phys. Lett.* 73(10), 1394-1396 (1998).
34. M. J. Montenegro, J. Lippert, S. Muller, A. Weidenkaff, P. R. Willmott and A. Wokaun, Pulsed laser deposition of electrochemically active perovskite films, *Appl. Surf. Sci.* 197, 505-511 (2002).
35. S. Müller, K. Striebel and O. Haas, $La_{0.6}Ca_{0.4}CoO_3$ - a Stable and Powerful Catalyst for Bifunctional Air Electrodes, *Electrochim. Acta* 39(11-12), 1661-1668 (1994).
36. S. Müller, F. Holzer, O. Haas, C. Schlatter and C. Comninellis, Development Of Rechargeable Monopolar And Bipolar Zinc Air Batteries, *Chimia* 49(1-2), 27-32 (1995).
37. S. Müller, O. Haas, C. Schlatter and C. Comninellis, Development of a 100 W rechargeable bipolar zinc/oxygen battery, *Journal Of Applied Electrochemistry* 28(3), 305-310 (1998).
38. T. Watanabe, A. Nakajima, R. Wang, M. Minabe, S. Koizumi, A. Fujishima and K. Hashimoto, Photocatalytic activity and photoinduced hydrophilicity of titanium dioxide coated glass, *Thin Solid Films* 351(1-2), 260-263 (1999).
39. J. G. Bednorz and K. A. Muller, Possible High-T_c Superconductivity In The Ba-La-Cu-O System, *Zeitschrift Fur Physik B-Condensed Matter* 64(2), 189-193 (1986).
40. F. S. Galasso, *Structure: Properties and Preparation of Perovskite-type Compounds*, (Pergamon Press, London, 1969).
41. H. Song, W. Kim, S. J. Kwon and J. Kang, Magnetic and electronic properties of transition-metal-substituted perovskite manganites-$La_{0.7}Ca_{0.3}Mn_{0.95}X_{0.05}O_3$ (X=Fe,Co,Ni), *J. Appl. Phys.* 89(6), 3398-3402 (2001).
42. J. T. Cheung, P. E. D. Morgan, D. H. Lowndes, X. Y. Zheng and J. Breen, Structural And Electrical-Properties Of $La_{0.5}Sr_{0.5}CoO_3$ Epitaxial-Films, *Appl. Phys. Lett.* 62(17), 2045-2047 (1993).

63. R. Srinivasan, Ablation Of Polymethyl Methacrylate Films By Pulsed (Ns) Ultraviolet And Infrared (9.17-Mu-M) Lasers - A Comparative-Study By Ultrafast Imaging, *J. Appl. Phys.* 73(6), 2743-2750 (1993).
64. T. Lippert, R. L. Webb, S. C. Langford and J. T. Dickinson, Dopant induced ablation of poly(methyl methacrylate) at 308 nm, *J. Appl. Phys.* 85(3), 1838-1847 (1999).
65. M. Hertzberg and I. A. Zlochower, Devolatilization Wave Structures And Temperatures For The Pyrolysis Of Polymethylmethacrylate, Ammonium-Perchlorate, And Coal At Combustion Level Heat Fluxes, *Combust. Flame* 84(1-2), 15-37 (1991).
66. T. Lippert, A. Yabe and A. Wokaun, Laser ablation of doped polymer systems, *Adv. Mater.* 9(2), 105-119 (1997).
67. H. Fukumura and H. Masuhara, The Mechanism Of Dopant-Induced Laser-Ablation - Possibility Of Cyclic Multiphotonic Absorption In Excited-States, *Chem. Phys. Lett.* 221(5-6), 373-378 (1994).
68. T. Lippert, J. Stebani, O. Nuyken, A. Stasko and A. Wokaun, Photolysis Of 1-Aryl-3,3-Dialkyltriazenes, *J. Photochem. Photobiol. A-Chem.* 78(2), 139-148 (1994).
69. O. Nuyken, J. Stebani, T. Lippert, A. Wokaun and A. Stasko, Photolysis, Thermolysis, And Protolytic Decomposition Of A Triazene Polymer In Solution, *Macromol. Chem. Phys.* 196(3), 751-761 (1995).
70. A. Stasko, V. Adamcik, T. Lippert, A. Wokaun, J. Dauth and O. Nuyken, Photochemical Decomposition Of Triazenes - (Electron-Paramagnetic-Resonance Study), *Makromolekulare Chemie-Macromolecular Chemistry And Physics* 194(12), 3385-3391 (1993).
71. T. Lippert, A. Wokaun, J. Stebani, O. Nuyken and J. Ihlemann, Dopant-Induced Laser-Ablation Of PMMA At 308-Nm - Influence Of The Molecular-Weight Of PMMA And Of The Photochemical Activity Of Added Chromophores, *Angew. Makromol. Chem.* 213, 127-155 (1993).
72. T. Lippert, L. S. Bennett, T. Nakamura, H. Niino, A. Ouchi and A. Yabe, Comparison of the transmission behavior of a triazeno-polymer with a theoretical model, *Appl. Phys. A-Mater. Sci. Process.* 63(3), 257-265 (1996).
73. T. Lippert, A. Wokaun, J. Stebani, O. Nuyken and J. Ihlemann, Triazene Polymers Designed For Excimer Laser Ablation, *Angew. Makromol. Chem.* 206, 97-110 (1993).
74. T. Lippert, J. Stebani, J. Ihlemann, O. Nuyken and A. Wokaun, Excimer-Laser Ablation Of Novel Triazene Polymers - Influence Of Structural Parameters On The Ablation Characteristics, *J. Phys. Chem.* 97(47), 12296-12301 (1993).
75. O. Nuyken, J. Stebani, T. Lippert, A. Wokaun and A. Stasko, Synthesis And Characterization Of Novel Triazeno-Group Containing Photopolymers, *Macromol. Chem. Phys.* 196(3), 739-749 (1995).
76. T. Lippert, T. Nakamura, H. Niino and A. Yabe, Irradiation wavelength selective surface modification of a triazeno polymer, *Macromolecules* 29(19), 6301-6309 (1996).
77. T. Lippert, T. Nakamura, H. Niino and A. Yabe, Laser induced chemical and physical modifications of polymer films: Dependence on the irradiation wavelength, *Appl. Surf. Sci.* 110, 227-231 (1997).
78. T. Lippert, E. Ortelli, J. C. Panitz, F. Raimondi, J. Wambach, J. Wei and A. Wokaun, Imaging-XPS/Raman investigation on the carbonization of polyimide after irradiation at 308 nm, *Appl. Phys. A-Mater. Sci. Process.* 69, S651-S654 (1999).
79. F. Raimondi, S. Abolhassani, R. Brutsch, F. Geiger, T. Lippert, J. Wambach, J. Wei and A. Wokaun, Quantification of polyimide carbonization after laser ablation, *J. Appl. Phys.* 88(6), 3659-3666 (2000).

97. H. Furutani, H. Fukumura, H. Masuhara, T. Lippert and A. Yabe, Laser-induced decomposition and ablation dynamics studied by nanosecond interferometry .1. A triazenopolymer film, *J. Phys. Chem. A* 101(32), 5742-5747 (1997).
98. M. Hauer, D. J. Funk, T. Lippert and A. Wokaun, Laser induced decomposition of a designed and a commercial polymer studied by ns-interferometry and shadowgraphy, *Appl. Phys. A-Mater. Sci. Process.* 77(2), 297-301 (2003).
99. M. Hauer, D. J. Funk, T. Lippert and A. Wokaun, *Proc. SPIE-Int. Soc. Opt. Eng.* 4760, 259 (2002).
100. T. Masubuchi, T. Tada, E. Nomura, K. Hatanaka, H. Fukumura and H. Masuhara, Laser-induced decomposition and ablation dynamics studied by nanosecond interferometry. 4. A polyimide film, *J. Phys. Chem. A* 106(10), 2180-2186 (2002).
101. T. Lippert, C. David, M. Hauer, T. Masubuchi, H. Masuhara, K. Nomura, O. Nuyken, C. Phipps, J. Robert, T. Tada, K. Tomita and A. Wokaun, Novel applications for laser ablation of photopolymers, *Appl. Surf. Sci.* 186(1-4), 14-23 (2002).
102. T. Lippert, A. Wokaun, S. C. Langford and J. T. Dickinson, Emission of neutral molecules during UV laser ablation of a photolabile triazeno polymer, *Appl. Phys. A-Mater. Sci. Process.* 69, S655-S658 (1999).
103. T. Lippert, S. C. Langford, A. Wokaun, G. Savas and J. T. Dickinson, Analysis of neutral fragments from ultraviolet laser irradiation of a photolabile triazeno polymer, *J. Appl. Phys.* 86(12), 7116-7122 (1999).
104. M. Hauer, T. Dickinson, S. Langford, T. Lippert and A. Wokaun, Influence of the irradiation wavelength on the ablation process of designed polymers, *Appl. Surf. Sci.* 197, 791-795 (2002).
105. J. T. Dickinson, J. J. Shin, W. Jiang and M. G. Norton, Neutral And Ion Emissions Accompanying Pulsed Excimer-Laser Irradiation Of Polytetrafluoroethylene, *J. Appl. Phys.* 74(7), 4729-4736 (1993).
106. G. P. Luo, Y. S. Wang, S. Y. Chen, A. K. Heilman, C. L. Chen, C. W. Chu, Y. Liou and N. B. Ming, Electrical and magnetic properties of $La_{0.5}Sr_{0.5}CoO_3$ thin films, *Appl. Phys. Lett.* 76(14), 1908-1910 (2000).
107. V. Craciun, D. Craciun, J. Perriere and I. W. Boyd, Droplet formation during extended time pulsed laser deposition of $La_{0.5}Sr_{0.5}CoO_3$ thin layers, *J. Appl. Phys.* 85(6), 3310-3313 (1999).
108. A. Gupta, B. W. Hussey and M. Y. Chern, Effect Of Different Oxidizing Gases On The Insitu Growth Of $YBa_2Cu_3O_7$-Delta Films By Pulsed Laser Deposition, *Physica C* 200(3-4), 263-270 (1992).
109. C. H. Chen, R. C. Phillips and M. P. McCann, Observation Of Trapped O_2 In High-T_c Metal-Oxide Superconductors, *Phys. Rev. B* 39(4), 2744-2747 (1989).
110. J. R. Engstrom and T. Engel, Atomic Versus Molecular Reactivity At The Gas-Solid Interface - The Adsorption And Reaction Of Atomic Oxygen On The Si(100) Surface, *Phys. Rev. B* 41(2), 1038-1041 (1990).
111. M. Cherry, M. S. Islam and C. R. A. Catlow, Oxygen-Ion Migration In Perovskite-Type Oxides, *Journal Of Solid State Chemistry* 118(1), 125-132 (1995).
112. Y. M. L. Yang, A. J. Jacobson, C. L. Chen, G. P. Luo, K. D. Ross and C. W. Chu, Oxygen exchange kinetics on a highly oriented $La_{0.5}Sr_{0.5}CoO_3$-delta thin film prepared by pulsed-laser deposition, *Appl. Phys. Lett.* 79(6), 776-778 (2001).
113. H. J. Dang and Q. Z. Qin, A thermal-controlling mechanism for laser ablation of a colossal magnetoresistant oxide target, *Chem. Phys. Lett.* 354(3-4), 210-216 (2002).

reviews.[3-9] The discussion about the mechanism of ablation started very soon after the discovery of ablation, and up to now no general agreement exists whether the mechanism is photochemical or photothermal. Recent papers[10] and reviews[11] favor a photothermal mechanism, but these studies are based on modeling of data for one polymer, i.e. Kapton™. This approach may be reasonable, but we should also not forget that there exists a long standing research topic, i.e. organic polymer photochemistry,[12] that has proven over many years that irradiation of organic molecules or polymers with UV photons will result in photochemical reactions. It is therefore very likely that also under ablation conditions, i.e. much higher fluences, photochemical reactions take place. The ablation products and the products of these photochemical reactions are related to the type of polymer and irradiation wavelength. Polymers may be classified for photon-induced reactions into polymers that depolymerize upon irradiation and into polymers that decompose into fragments. The assignment of the polymers to one of these two classes is closely related to the synthesis of the polymer: polymers that are formed by radical polymerization from monomers which contain double bonds are classical candidates for depolymerization upon irradiation, while polymers that are formed by reactions such as polycondensation will not decompose into the monomers upon irradiation. This means of course also that no films with the same chemical structure and/or molecular weight can be obtained by pulsed laser deposition from these polymers as targets. A possible exception may be a process termed resonant infrared pulsed laser deposition (RIR-PLD)[13] where a tunable IR laser, i.e. a free electron laser, is applied as irradiation source. Other processes, such as MAPLE (matrix-assisted pulsed laser evaporation)[14] or RIR-MAPLE[15] may be utilized to form polymer films with intact structures of the films and without any pronounced degradation of the polymer. More common than the deposition of organic or polymeric films is the laser deposition of metallic or ceramic films, which will be discussed for selected oxides films below.

1.2. PULSED LASER DEPOSITION OF METAL OXIDES

For the deposition of thin metal or ceramic films various methods can be applied, such as molecular beam epitaxy (MBE),[16] chemical vapor deposition (CVD),[17] sputtering (RF, Magnetron, and ion beam),[18] and pulsed laser deposition (PLD).[19-21] The advantages of PLD compared with other deposition techniques are well summarized by Chrisey and Hubler.[22] Briefly, the main advantage of PLD is the flexibility to control different parameters which allows an optimization of the deposition conditions. The arrival rates of atoms on the substrate and the possibility to work with

propagate freely away from the localized scattering region.[23] The advantages of PRCLA compared to PLD were demonstrated by Willmott and Antoni[33] for the growth of GaN films. PRCLA has also been applied successfully[34] for the growth of perovskite films. The films present the desired oxygen content without any post-annealing procedure.

The optimization of the different deposition parameters during the growth of $La_{0.6}Ca_{0.4}CoO_3$ thin films, and its influence on the electrochemical performance for the oxygen evolution/reduction reaction, are presented in this chapter. The specific material composition was selected due to its industrial application as bifunctional catalyst in electrically rechargeable Zn/air batteries.[35-37]

1.2.1. *Selected Oxides: Perovskites and Li-Spinels*

Metal oxides constitute a fascinating class of materials whose properties cover the entire range from metals to semiconductors and insulators. Their surfaces play a crucial role in several processes, i.e. passivation of metal surfaces against corrosion, catalysis for the partial oxidation of hydrocarbons, and the stability of electrode/electrolyte interfaces in fuel cells.

In spite of all their technological and scientific importance, our understanding of the basic physics and chemistry of metal-oxide surfaces lags a decade or more behind that of other metals and semiconductors. However, over the past twenty years, an increasing number of groups have begun to study the properties of transition metal oxides for novel applications. For example in catalysis stimulated by the discovery of TiO_2 as a catalytic electrode in a photoelectrolysis cell, which decomposes water into H_2 and O_2, without the application of an external voltage[38] or by the discovery of Cu-oxide-based high T_c superconductors.[39]

Metal oxides, with an empirical formula ABO_3, derive their name from the mineral "perovskite", with the chemical structure $CaTiO_3$. The cubic form of this material is referred to as ideal perovskite, and has a unit cell edge of approximately 4Å. In reality, only a few perovskite-type materials have this ideal cubic structure at room temperature, but many reach it at higher temperatures.[40] Distortions from the cubic symmetry produce tetragonal, orthorhombic, and rhombohedral structures as shown in Fig. 2. In the face centred cubic (FCC) structure the *A cations* are located at the corners while the O atoms are on the faces. The *B cation* is in the centre of the unit cell.

challenging task. Only few catalysts are intrinsically bifunctional to act as catalysts for both oxygen reactions. Most of the catalysts exhibit either a low catalytic activity or they are unstable under operating conditions.[46,47] The perovskites containing Co, Fe, Mn and Ni are excellent catalysts for the oxygen evolution (OER) and oxygen reduction reaction (ORR).[48,49] The origin of the catalytic activity is not yet fully understood and the different preparation methods are one reason for conflicting results. The best method to overcome this influence is the preparation of electrodes on inactive substrates with well defined electrolyte/oxide interfaces, i.e. model systems. This will allow to study and compare the mechanism of the oxygen reduction/evolution reaction of different perovskite oxides without any interference from the carbon support material. Another advantage of the model system is the possibility to study the influence of the crystallographic orientation on the catalytic activity. The best model system will therefore be a dense crystalline films deposited on an inactive substrate, which can be prepared by pulsed laser deposition.

Another class of oxides that play a major role for batteries, but in the case of lithium-batteries, is the lithium spinels. The ideal spinel oxide structure is AB_2O_4 where the oxygen atoms form a face-centered cubic packing and occupy 32*e* sites of the space group Fd3m. The cations A and B occupy the tetrahedral 8*a* sites and the 16*d* sites respectively, whereas the octahedral site 16*c* remains empty. The spinel structure is illustrated in Figure 3.

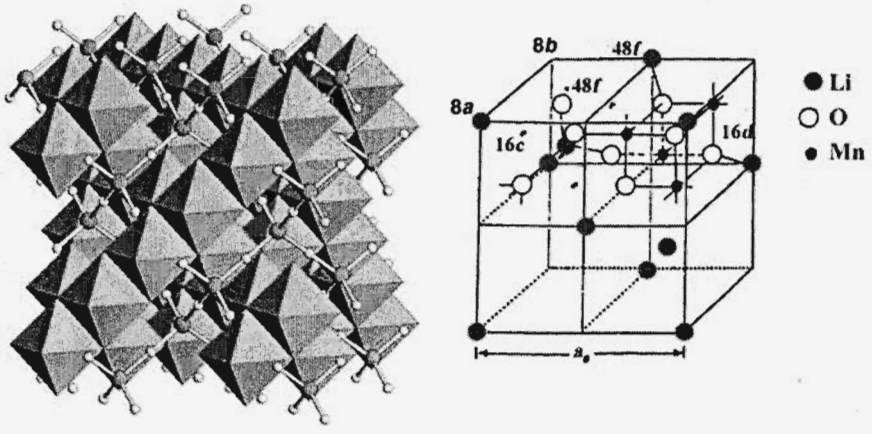

Figure 3. Crystal structure of spinel phase, general (left) and for $LiMn_2O_4$ (right). Adopted from [60].

For cathode electrode materials, suitable lithium spinels oxides are generally of the form LiM_2O_4 (with M: transition Metal such as Mn and

the Li-ions due to the formation of Mn^{4+} sites. Extraction of Lithium from sites in the neighborhood of Mn^{4+} sites requires more energy, which is the reason for the pronounced two steps Li extraction. The two peaks at 3.99 and 4.1 V (at negative currents) correspond to the reintercalation of lithium upon discharge.

2. Results and Discussion

2.1. ABLATION OF POLYMERS

2.1.1. *Classification of Polymers for Laser Ablation*

A typical example for a polymer that depolymerizes, i.e. forming the monomer, is poly-methylmethacrylate (PMMA), while typical examples for polymers that decompose into fragments are polycarbonates and polyimides. These polymers are formed by the reaction of the monomers where HCl or H_2O are formed as products. These polymers will decompose upon irradiation with photons in some fragments that cannot be identical with the monomers.

In the case of PMMA decomposition into the monomer is possible, but a complete transformation is only possible for a pure thermal degradation with temperatures above the ceiling temperature, T_C ($\approx$ 280 °C), of PMMA. The ceiling temperature is defined as the temperature where the equilibrium between the polymer and monomer is totally on the side of the monomer, but analysis of the ablation products upon irradiation with UV wavelengths reveals that only a small amount, i.e. $\approx$ 1% for 248 nm irradiation and $\approx$ 18% for 193 nm irradiation[62,63] of the products is the monomer. The detected products are at least partially compatible with the well-known products of the photolysis of PMMA. The photodecomposition starts with the excitation of monomer unit, where for 248 nm irradiation the $n \rightarrow \pi^*$ transition of the ester group is excited. The following steps are the side chain scission of the ester group which is followed by hydrogen abstraction by the radicals, and elimination of CO or CO_2. The initial reaction, i.e. the bond scission next to the carbonyl group is one of the most prominent photochemical reactions, known as Norrish type I reaction or α-cleavage. The successive steps are the main chain scission which is accompanied by the creation of double bonds (chain end and mid chain) which is also detected during UV laser irradiation of PMMA.[64] These reactions create a modified polymer and the process has been termed photo-yellowing for low photon fluxes, e.g. sunlight, and incubation for ablation conditions. Incubation describes the chemical and physical changes in the polymer prior to ablation, i.e. mainly an increase of the absorption at the irradiation

i.e. mainly nitrogen, was detected. The quality of the ablation structures is not satisfying due to the high roughness in the ablation craters, the ill-defined rims, and the large amount of ablation products surrounding the structures. One reason for these features could be the low amount of dopants and the corresponding low absorption coefficients of the doped polymers. Doping of polymers with small molecules is unfortunately limited because it is only possible to dope polymers with up to ≈ 10 wt.-% which is already accompanied by a clear decrease of the glass transition temperatures of the polymers. Higher doping levels can also result in an agglomeration of the dopant, which may cause inhomogeneous ablation. Therefore, new polymers were developed which had the photolabile triazene group in the polymer main chain, with two triazene chromophores in each repetition unit. This approach has several distinct advantages:

- the possibility to evaluate the influence of photochemical reactions on the ablation properties by tailoring the polymer;
- the chance to overcome some of the drawbacks of laser ablation that are normally observed for standard polymers. These drawbacks are the pronounced carbonization of the ablated surface and the redeposition of ablation products in the vicinity and inside the ablation craters.

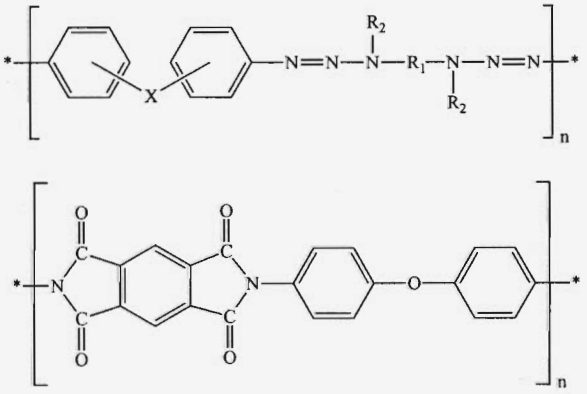

Figure 5. Chemical structures of the triazene polymers (TP) and of polyimide (Kapton™).

The designed triazene-polymers, TP, (general structural unit shown in Figure 5 top) reveal several unique features. The absorption maximum and absorption coefficient can be tuned to certain wavelengths by varying "X" in Figure 5.[69] This allows to match their absorption coefficients to other polymers that are used for comparison, e.g. polyimide, Kapton™ (structure shown in Figure 5 bottom). The absorption maximum of the TP can be tuned from 290 to 360 nm with maximum linear absorption coefficients,

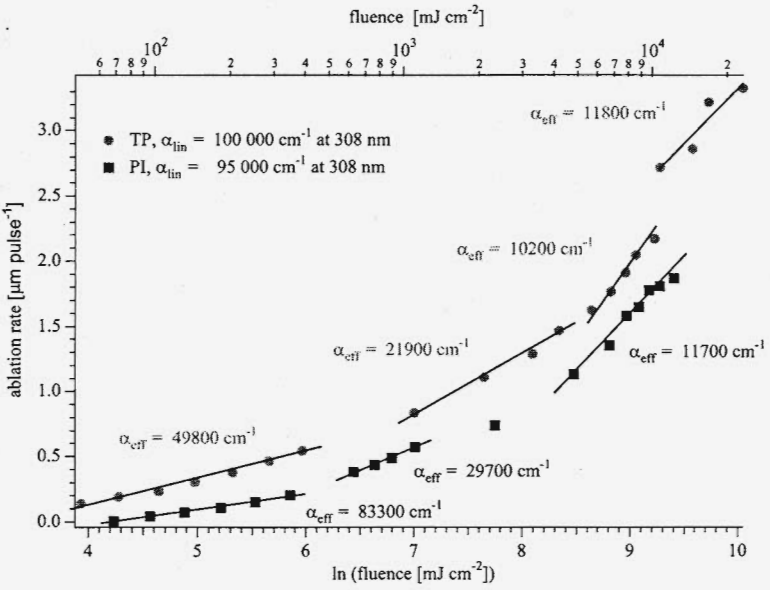

Figure 8. Ablation rates versus laser fluence for TP1 and Kapton™, including the linear fits according to equation 1 to obtain the effective absorption coefficients, α_{eff}.

The effective absorption coefficient, α_{eff} was calculated according to equation 1 (see below). Both polymers reveal a quite complex ablation behavior, which may be described by several linear relations which indicate changes of the ablation process or mechanisms. The linear ranges can be used to calculate α_{eff} which suggest in the case of TP and also for PI (Kapton™) that in the whole fluence range a pronounced bleaching is observed (lower α_{eff} than α_{lin}).[73-75] This results in larger laser penetration depths and therefore higher ablation rates than predicted by the absorption coefficients. This bleaching process is more pronounced for TP in the low fluence range than for PI, but increases for both polymers with increasing fluences. At the highest fluences this trend seem to change in the case of TP, where a slight increase of α_{eff} is observed, which is assigned to plasma absorption (plasma shielding).[74] The differences between the two polymers in the low fluence range are most probably due to the more efficient photochemical decomposition of the TP during the laser pulse. Another interesting difference between these polymers is the quality of the ablated structures. The TP can be structured at this irradiation wavelength with high quality and without any visible redeposited ablation product or modification of the abated polymer surface. The pictures in Figure 9 show the comparison of a test pattern ablated into TP (left) and Kapton™.

The usual way to obtain these values is by applying the following empirical equation[80,81] to the ablation rates:

$$d(F) = \frac{1}{\alpha_{eff}} \ln\left(\frac{F}{F_{th}}\right)$$

The ablation rate per pulse, d(F), is plotted as function of the logarithm of the laser fluence, F, and from the linear fits the threshold fluence, F_0, and the effective absorption coefficient, α_{eff}, are obtained. The first fundamental issue is the ablation rate per pulse, and whether this is defined as an ablation rate for a single pulse, or as the slope of a plot where the ablation depth is plotted as function of the pulse numbers for a given fluence. These two different analytical methods can result in very different ablation rates, especially in the case of polymers which reveal incubation. Incubation is defined as the processes that are often accompanied by an increase of absorption, e.g. due to the double bonds in PMMA and which take place during irradiation or prior to the onset of ablation. This means for ablation that a certain number of pulses are not inducing ablation, but only chemical or physical modification of the polymer. If the ablation rates include these incubation pulses, then of course different ablation rates are obtained then for an analysis where only the pulses are used for which ablation is detected. Another problem in analyzing the ablation depth from multipulse experiments is the above described surface modification of the polymer which may alter the ablation rates with consecutive pulses. These difficulties can be overcome by utilizing only single pulse ablation rates, which are of course more difficult to measure, as very sensitive techniques are needed. Unfortunately even one problem may be encountered for single pulse experiments which originates from an experimental procedure where consecutive pulses are delivered to the same position of the polymer. In the case of polyimide[82,83] and several other polymers chemical modifications are detected, which corresponds very often to carbonization of the polymer. The polymer with this carbonized layer exhibits a different ablation rate, due to the different material properties of this composite material, which are not comparable to the original polymer. It is also necessary to consider that also physical changes of the polymer surface, i.e. an increase of roughness, can cause problems. An increase of roughness corresponds also to an increase of the surface area, which results in an decrease of laser fluence that can even terminate ablation when the fluence decreases below the ablation threshold.[84] True single pulse experiments may also encounter a problem originating from the sample preparation, if solvent based techniques are used. A dense skin layer may be formed, which can exhibit different ablation rates, i.e. lower rates, than the bulk material that contains also remaining solvent. The last point that has to be considered is the

irradiation. The triazene-chromophore decomposes at fluences well below the ablation threshold and is clearly the most sensitive chromophore in the triazene-polymer that decomposes directly during 308 nm irradiation. The ablation data suggest also that the photochemical activity and therefore also the possibility of a photochemical part in the ablation mechanism is at least likely.

Therefore one triazene polymer, i.e. TP (Figure 7) was selected for analysis by various time-resolved techniques during and directly after irradiation at 308 nm and 248 nm. The following techniques have been applied to probe the ablation mechanism:

- Time resolved transmission
- Ns shadowgraphy
- Ns surface interferometry and
- Time-of-flight mass spectrometry.

In an attempt to account for the different ablation behavior at 308 and 248 nm, i.e. the different surface modification[76,77] and the lower ablation rates for 248 nm irradiation,[73] time resolved transmission experiments were performed. An increase in transmission with increasing fluences was observed for 248 and 308 nm irradiation, suggesting the presence of a bleaching process at higher fluences.[72,90] In principle, this bleaching could be transient or permanent (=decomposition). A higher degree of bleaching was detected for 308 nm irradiation which can account for the higher ablation rates at this wavelength. To address the issue of a possible photothermal contribution to the ablation mechanism, a nanosecond imaging technique[91-94] was employed that produces a series of shadowgraphs of the air-polymer interface. Two different experimental techniques were employed, which have been described in detail elsewhere.[95] Only a very pronounced shockwave in air was detected which also confirms the absence of solid products for 308 nm irradiation. The advance of the supersonic shock waves can be modeled by a model of the blast wave which incorporates the mass of the ablated polymer and the decomposition enthalpy of the polymer. Shadowgraph imaging was supplemented by ns-surface interferometry.[93,96,97] Interferometric images (shown in Figure 10) can reveal changes in surface morphology on ns-timescales, both during and after the laser pulse. Some of these changes are potentially related to photochemical and photothermal ablation mechanisms: photothermal ablation is often associated with a pronounced surface swelling and delayed material ejection, while photochemical ablation is expected to yield instantaneous etching. Interferometric images of TP at 193, 308[98,99] and 351 nm[97] show that etching of the film begins and ends with the laser pulse (shown in Fig. 10 for 308 nm irradiation). In

in Figure 11),[89,102,103] but it is also a fact that thermal decomposition yields similar products.[69]

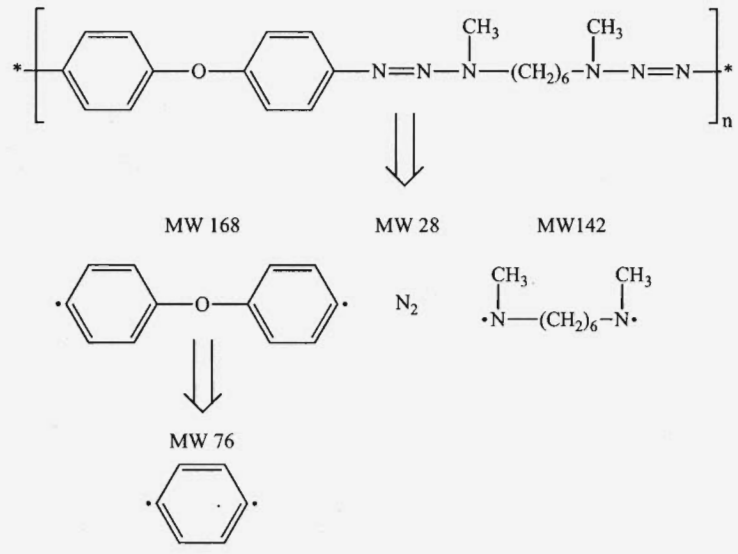

Figure 11. Decomposition pathway for TP1 and 308 nm irradiation with all fragments that were observed in TOF-MS measurements.

Importantly, three different species of nitrogen were detected in the TOF-signals (shown in Figure 12), including a very fast ground state neutral (up to 6 eV of kinetic energy), a slower neutral ground state species with a broad energy distribution (probably a thermal product), and possibly a metastable (excited) neutral N_2 species.[104] The latter can only be created by an electronic excitation. The time of flight curves for a commercial polymer, i.e. Teflon™, after irradiation at 248 nm reveals unzipping, where the main product of decomposition is the monomer (mass 100, C_2F_4). The TOF curve was modeled by a Maxwell-Boltzman distribution which yields a temperature of 710 °C that is at least compatible with the decomposition (> 400 °C) and ceiling temperature (≈ 930 °C) of Teflon.[105]

The data for the photochemical active triazene polymer (TP) suggest strongly that photochemistry can play an important role in the ablation mechanism of polymers, but it is also clear that photothermal induced reactions are also important. This is for example confirmed by the presence of a thermal N_2 product in the TOF curves. A photothermal mechanism will always be present, especially if the polymers decompose exothermically during photochemical decomposition and if the quantum yields of the photochemical reactions is not equal to 1.

clusters. These subcritical clusters tend to dissociate into mobile species that will nucleate during the time of no vapour arrival into new clusters of a different size. The next pulse will initiate the same process again, with the difference that some of the mobile atoms will reach the previous formed clusters. There are a number of changes in the film growth mode that are readily observed as a function of the PLD parameters (wavelength, fluence, repetition rate, and pulse width). Table 1 presents a summary of different deposition parameters and the effect on the film growth.[22]

Table 1. Relationship between deposition parameters and film characteristics.

Category	Parameters	Effect on process	Possible effect on film
Primary	Laser Wavelength Laser Power Density	Thermal or nonthermal evaporation	Control of compositional variation and transfer ratio
	Laser Repetition Rate	Ratio of neutral to ionic species in the plasma Kinetic energy of the ejected species	Formation of metastable structures Particulates
Secondary	Substrate temperature	Mobility of ablated species on the substrate	Formation of metastable structures
	Oxygen partial pressure	Reactive oxygen species	Oxygen content of film, Epitaxial growth Control of crystal structure
Tertiary	Substrate-target distance	Plume density near the substrate	Film Thickness

2.2.2. *Effect of the Different Oxygen Sources*

The presence of an oxygen background during the film growth is one of the most important aspects to avoid oxygen deficient films. It has been suggested by Craciun et al.[106] that prolonged laser ablation of $La_{0.5}Sr_{0.5}CoO_3$ (LSCO) causes preferential oxygen evaporation in the target, which results in volume absorption and explosive volume boiling, causing the ejecting of droplets from the target[107]. This is not the case for the very similar LCCO compound ($La_{0.6}Ca_{0.4}CoO_3$) using PRCLA as deposition technique, where even after 2×10^6 pulses to the target no changes in the film quality and composition (also of the target) were observed. LCCO-Films grown in an O_2 background are dark and mirror like, independent of the cooling

$8x10^{-4}$ mbar background, as compared to the flux of liberated target atoms created by laser ablation. The kinetic requirement for stoichiometric oxide growth is therefore not fulfilled (to produce an effective oxidation of the cationic species), resulting in films with an oxygen deficiency. With the synchronized N_2O gas pulse, an excess of oxygen atoms (originating from the dissociation of N_2O by collisional fragmentation with the plasma species, or electron-impact[108]) is created, and the species from the LCCO target arrive simultaneously at the substrate, resulting also in films with oxygen deficiency. The films with the best oxygen stoichiometry are obtained when both oxidizing sources are applied. To understand these results we have to consider not only the arrival time of the particles at the substrate, but also the time between each pulse. There exists an oxygen diffusion equilibrium that influences the oxygen content of the growing film[111,112]. This equilibrium is partially shifted due to loss of oxygen from the film, when only the background is present ($8x10^{-4}$ mbar of oxygen). In the case of the N_2O pulse only, there is more reactive oxygen present leading to the desired oxygen partial pressure during the arrival of the atoms at the substrate. The low background of 2×10^{-6} mbar and the absence of additional oxygen between the pulses will shift the diffusion equilibrium even further in the direction of "out diffusion". When both the N_2O pulse and the additional oxygen background are applied, a large number of oxygen atoms will arrive together with the species originated from the target at the substrate. There is now more oxygen available between the pulses, which minimizes the loss of the volatile oxygen from the surface. Therefore the films with the highest oxygen content are obtained when a gas pulse and background pressure are applied.

2.2.3. *Influence of the Substrate Temperature – Distance Between Target-Substrate*

The substrate temperature not only determines the initial growth of a film, but its subsequent growing as well, and therefore determining its microstructure. In general, the best value of substrate temperature corresponds to the regime where there is sufficient surface diffusion to allow surface atoms to minimize their surface energy to reach thermodynamically stable sites.

The velocity and the kinetic energy of selected neutral and charged ablation species produced by PRCLA are compiled in Table 3. The data are obtained from time- and space-resolved emission spectroscopy. The low kinetic energy of these species arriving at the substrate compared to PLD[113] is due to the large number of collisions with the gas pulse molecules, which occur in the initial interaction zone (around 10 times more collisions than

The crystallographic orientations of the grown films as a function of target-substrate distance and substrate temperature are shown in Fig. 13. For a given temperature (e.g. 650 °C) and a variable target-substrate distance the films are only oriented in the (100) direction (same as the substrate) for distances up to approximately 4.7 cm; while for larger distances a mixture of (100/110) orientations is observed. A change in the orientation is also observed when the distance is kept at 4.5 cm and the temperature is increased from 550 to 700 °C. At lower temperatures a mixture of the (100/110) orientation is observed, while at higher temperatures only the (100) orientation is present. Amorphous films can be obtained at low temperatures and large distances. This control of crystallinity can be explained by the kinetic energy of the arriving particles at the substrate surface. Two energy sources are important during PLD film growth, i.e. the kinetic energy of the arriving particles and the substrate temperature, and influence therefore the crystallographic structure and film morphology. The substrate temperature is determining the crystallographic orientation when the distance (kinetic energy) is kept constant. An increase of the temperature improves the surface mobility of the clusters and atoms arriving at the substrate. In this case the number of defects is minimized (due to the surface mobility) and the film growth in the orientation of the substrate. The transition temperature from mixed orientation to epitaxial film growth is observed at higher temperatures when the target-substrate distance is increased (to e.g. 5 cm), yielding lower kinetic energies of the arriving species. This behaviour, i.e. the synergetic effect of the energy from substrate temperature and kinetic energy, is confirmed by the corresponding experiments where the temperature is kept constant while the distance is varied. The transition of mixed orientation to single crystalline is now observed when the distances are decreased. The variation of these two parameter (distance and temperature), gives the unique opportunity to prepare films with crystallographic features that vary from amorphous to epitaxial without changing the pressure of the background gas or the substrate.

2.2.4. *Electrochemical Characterization of Thin Films vs. Gas Diffusion Electrodes*

The comparison between gas diffusion and thin films will only be discussed briefly. An electrochemical process involves several steps, i.e. mass transfer, chemical reaction, adsorption/desorption, and electron transfer. The mass transfer of oxygen from the solution to the electrode surface is assumed to be the same for both electrode types. For the last two steps a pronounced difference exists between the gas diffusion and the thin film

example is the difference in cyclic voltammograms for the adsorption/desorption of hydrogen on the different surfaces of platinum.[116]

The importance of the crystallinity on several electrochemical reactions and the fact that until now the studies for the oxygen evolution/reduction on LCCO were only performed on polycrystalline gas diffusion electrodes were one of the driving forces to perform experiments using thin LCCO films with different crystallographic orientations. Only for dense films will the observed catalytic activity correspond to the catalyst and the active area of the electrode can be easily determined and compared to other electrodes.

The polarization curves for thin amorphous, mixed, and single crystalline LCCO films are compared in Fig. 14.

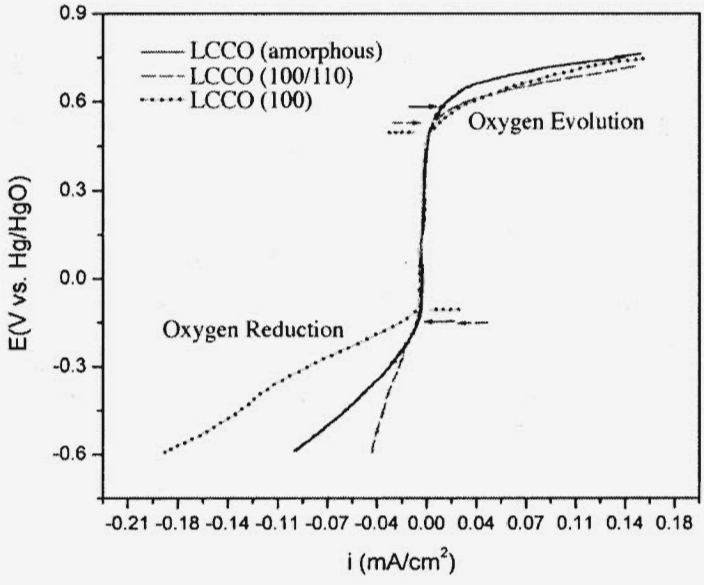

Figure 14. Polarization curves of amorphous, single- and polycrystalline LCCO thin films deposited on MgO(100) substrates.

The polarization curves show that the crystallinity influences directly the catalytic activity for oxygen reduction and evolution reactions (measured by the overpotential). The overpotential is the difference between the values indicated with the arrows in Fig. 14. The film with the smallest overpotential (597 mV) is the (100) oriented sample followed by the film with mixed 110 and 200 orientation (679 mV) and the amorphous film (738 mV). An electrochemical process, as discussed previously, involves several steps, i.e. mass transfer, chemical reaction, adsorption/desorption, and electron transfer. The result indicates that the only step that can influence the electrochemical behaviour of these three

Fig 16 shows the cyclic voltammogram of a $LiMn_2O_4$ film deposited on polished titanium foil under the same conditions. The film is roughly 0.7 μm thick.

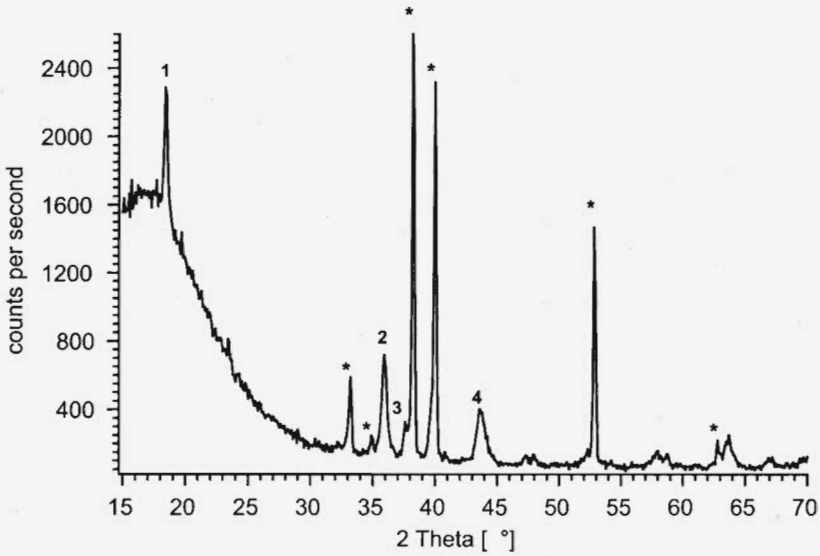

Figure 15. XRD spectrum of a $LiMn_2O_4$ (nominal composition) film deposited on a titanium substrate. The signals that can be attributed to a spinel structure are: 18.4° for the (111) (1), 35.6° for the (311) (2), 37.78° for the (222) (3) and 43.6° for the (004) (4) orientation. The peaks marked with an asterisk can be assigned to the titanium substrate.

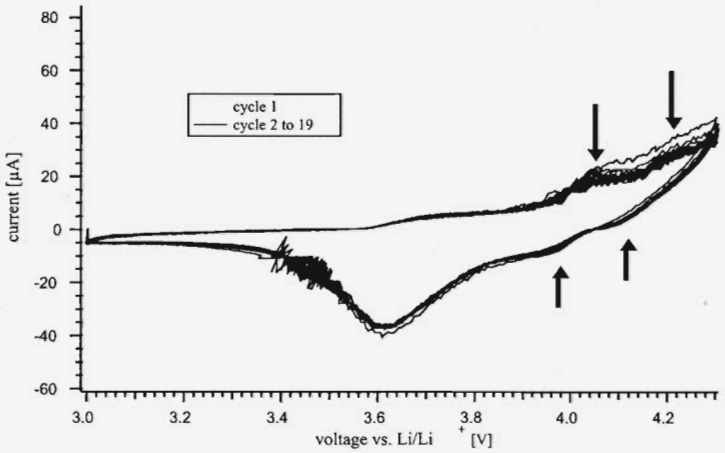

Figure 16. Cyclic Voltammogram of a $LiMn_2O_4$ (nominal composition) film deposited on a titanium substrate at a distance of 3 cm from the target.

Morcrette et al.[117,123] have shown that there is a small window for the oxygen background pressure that can be used for the stoichiometric deposition of $LiMn_2O_4$. The group analyzed $LiMn_2O_4$ films deposited on polycrystalline platinum substrates by PLD from a stoichiometric target. The oxygen pressure was varied between 10^{-6} and 1 mbar while the temperature was varied between 300 and 700°C.[117,123] A quadrupled Nd:YAG laser with a wavelength of 266 nm, 5 Hz repetition rate and with a fluence of 2 J/cm^2 was applied for these experiments. No post-deposition annealing was performed to eliminate the possibility of compositional changes in the film. The results indicate that a low background pressure results in lithium deficient films. This is most probably due to the low vapor pressure of Lithium oxide which could evaporate at lower oxygen background pressure and higher substrate temperatures.

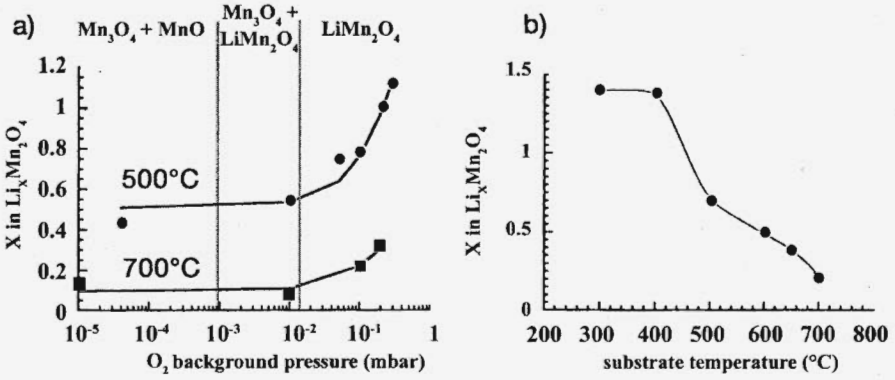

Figure 18. (a) RBS analysis of the Li stoichiometry coefficient as a function of the oxygen pressure for two temperatures 500°C (top curve) and 700°C (bottom curve), (b) RBS analysis of the Li stoichiometry coefficient as a function of temperature for the pressure of 0.1 mbar. Adopted from [117].

The higher oxidation states of manganese, such as Mn^{3+} in $Li_xMn_2O_4$ are not formed in the film since lower oxidation states, such as Mn^{2+} are favored.[117] In Fig. 18 the RBS analysis of the Li/Mn ratio as a function of oxygen pressure and substrate temperature is shown, which reveals a manganese deficiency due to high background pressure.[123] The optimized pressure for obtaining a $LiMn_2O_4$ spinel phase is 0.2 mbar while the optimum temperature for 0.1 mbar of pressure is 450 °C (Fig. 18b). The electrochemical characterization, i.e. cyclic voltammogram, of these films correspond to what is expected from $LiMn_2O_4$.[117,123] Experiments performed at different target/substrate distances between 3 and 7 cm and background pressures between 0.1 and 0.3 mbar support these results.[126] XRD

lithium deficiency in the films is also a result of preferential resputtering of Li caused by the fast ionic species in the plasma which are sufficiently slowed down by the molecules of the background gas at higher pressures.

3. Conclusion

Laser ablation of polymers is an established technique in various industrial applications and the large number of studies published annually indicate that this is still an attractive area of research. Discussions above the ablation mechanisms are ongoing and will continue to be one of the topics in ablation of polymers. The development of polymers designed specifically for laser ablation is a unique tool for probing the ablation mechanisms as well as for improving ablation properties. New commercial applications will require improved ablation rates and control of undesirable surface effects, such as debris. The complexity of interactions between polymers and laser photons are illustrated by the various processes associated with different irradiation conditions, e.g for short pulses, high repetition rates, CW irradiation, etc.. The ongoing maturation of laser techniques will increase the number of applications of laser ablation in the future. In the last decade we have seen the development of several exciting laser ablation tools, including femtosecond lasers, VUV lasers, free electron lasers, and high repetition-rate lasers. All these new techniques are applied in ongoing research in conjunction with a variety of analytical techniques. Femtosecond lasers and VUV lasers in particular are expected to lead to important industrial applications. The simultaneous development of various VUV sources for large area irradiation, such as excimer or resonance lamps, will also result in a steady increase of applications and a better understanding of photon induced processes in polymers.

The application of PRCLA as deposition technique allows the preparation of thin films of perovskite-type oxide materials with a nearly completely filled oxygen sublattice and without additional processing steps (e.g. annealing). The low kinetic energy of the atoms/species arriving at the substrate surface prevents re-sputtering, which yields films with the same composition as the target material, for a variety of target-substrate distances. The crystallinity of the films can be controlled from amorphous to single crystalline, by varying the substrate temperature, the substrate and its orientation, and the distance between target and substrate. Our studies have revealed that the crystallinity has a pronounced influence on the catalytic activity. The films produced by PRCLA prove the possibility to apply thin films as model systems for electrochemical studies. Epitaxial films of LCCO reveal a higher activity than films with mixed orientation, followed by amorphous films.

7. T. Lippert and J. T. Dickinson, Chemical and spectroscopic aspects of polymer ablation: Special features and novel directions, *Chem. Rev.* 103(2), 453-485 (2003).
8. T. Lippert, in: Polymers And Light, (Springer-Verlag Berlin, Berlin, 2004), pp. 51-246.
9. N. Bityurin, Studies on laser ablation of polymers, *Annu. Rep. Prog. Chem., Sect. C* 101, 216-247 (2005).
10. N. Arnold and N. Bityurin, Model for laser-induced thermal degradation and ablation of polymers, *Appl. Phys. A-Mater. Sci. Process.* 68(6), 615-625 (1999).
11. N. Bityurin, B. S. Luk'yanchuk, M. H. Hong and T. C. Chong, Models for laser ablation of polymers, *Chem. Rev.* 103(2), 519-552 (2003).
12. J. F. Rabek, *Mechanism of Photophysical Processes and Photochemical Reactions in Polymers*, (John Wiley & Sons, 1987).
13. D. B. Chrisey, A. Pique, R. A. McGill, J. S. Horwitz, B. R. Ringeisen, D. M. Bubb and P. K. Wu, Laser deposition of polymer and biomaterial films, *Chem. Rev.* 103(2), 553-576 (2003).
14. A. Pique, R. A. McGill, D. B. Chrisey, D. Leonhardt, T. E. Mslna, B. J. Spargo, J. H. Callahan, R. W. Vachet, R. Chung and M. A. Bucaro, Growth of organic thin films by the matrix assisted pulsed laser evaporation (MAPLE) technique, *Thin Solid Films* 356, 536-541 (1999).
15. B. Toftmann, M. R. Papantonakis, R. C. Y. Auyeung, W. Kim, S. M. O'Malley, D. M. Bubb, J. S. Horwitz, J. Schou, P. M. Johansen and R. E. Haglund, UV and RIR matrix assisted pulsed laser deposition of organic MEH-PPV films, *Thin Solid Films* 453-54, 177-181 (2004).
16. H. S. Wang, D. Eissler, Y. Kershaw, W. Dietsche, A. Fischer, K. Ploog and D. Brunner, New Crucible Made Of Y_2O_3 For Preparing Yttrium Based High-T_c Superconducting Films By Molecular-Beam Epitaxy, *Appl. Phys. Lett.* 60(6), 778-780 (1992).
17. C. Dubourdieu, M. Rosina, H. Roussel, F. Weiss, J. P. Senateur and J. L. Hodeau, Pulsed liquid-injection metalorganic chemical vapor deposition of $(La_{0.7}Sr_{0.3}MnO_3/SrTiO_3)(15)$ superlattices, *Appl. Phys. Lett.* 79(9), 1246-1248 (2001).
18. T. G. S. Cruz, M. U. Kleinke and A. Gorenstein, Evidence of local and global scaling regimes in thin films deposited by sputtering: An atomic force microscopy and electrochemical study, *Appl. Phys. Lett.* 81(26), 4922-4924 (2002).
19. V. G. Prokhorov, Y. P. Lee, K. W. Kim, V. M. Ishchuk and I. N. Chukanova, Long-aging effects on the properties of $La_{0.5}Sr_{0.5}CoO_3$-delta films, *Appl. Phys. Lett.* 80(13), 2353-2355 (2002).
20. F. J. Cadieu, L. Chen, B. Li and T. Theodoropoulos, Enhanced room temperature magnetoresistance response in textured $La_{0.7}Sr_{0.3}MnO_3$ strips made by pulsed laser deposition, *J. Appl. Phys.* 87(9), 6770-6772 (2000).
21. R. Rauer, J. Backstrom, D. Budelmann, M. Kurfiss, M. Schilling, M. Rubhausen, T. Walter, K. Dorr and S. L. Cooper, Thickness dependent phase separation in $La_{0.7}Ca_{0.3}MnO_3$ films, *Appl. Phys. Lett.* 81(20), 3777-3779 (2002).
22. D. B. Chrisey and G. K. Hubler (eds.), *Pulsed Laser Deposition of Thin Films*, (John Wiley & Son, New York, 1994).
23. P. R. Willmott and J. R. Huber, Pulsed laser vaporization and deposition, *Reviews Of Modern Physics* 72(1), 315-328 (2000).
24. T. Kobayashi, H. Akiyoshi and M. Tachiki, Development of prominent PLD (Aurora method) suitable for high-quality and low-temperature film growth, *Appl. Surf. Sci.* 197, 294-303 (2002).
25. A. Giardini, V. Marotta, A. Morone, S. Orlando and G. P. Parisi, Thin films deposition in RF generated plasma by reactive pulsed laser ablation, *Appl. Surf. Sci.* 197, 338-342 (2002).

43. S. Müller, F. Holzer and O. Haas, Optimized zinc electrode for the rechargeable zinc-air battery, *Journal Of Applied Electrochemistry* 28(9), 895-898 (1998).
44. B. D. McNicol and A. A. J. Rand, *Power Sources for Electric Vehicles*, (Elsevier, Amsterdam, 1984).
45. I. Buchmann, *Batteries in a portable world*, (Cadex Electronics, Richmond, 2001).
46. J. Prakash, D. Tryk and E. Yeager, Electrocatalysis For Oxygen Electrodes In Fuel-Cells And Water Electrolyzers For Space Applications, *J. Power Sources* 29(3-4), 413-422 (1990).
47. J. Prakash, D. Tryl, W. Aldred and E. Yeager, *Electrochemistry in Transition*, (Plenum Press, New York, 1992).
48. R. N. Singh, N. K. Singh and J. P. Singh, Electrocatalytic properties of new active ternary ferrite film anodes for O_2 evolution in alkaline medium, *Electrochim. Acta* 47(24), 3873-3879 (2002).
49. T. Horita, K. Yamaji, N. Sakai, H. Yokokawa, A. Weber and E. Ivers-Tiffee, Oxygen reduction mechanism at porous $La_{1-x}Sr_xCoO_{3-d}$ cathodes/$La_{0.8}Sr_{0.2}Ga_{0.8}Mg_{0.2}O_{2.8}$ electrolyte interface for solid oxide fuel cells, *Electrochim. Acta* 46(12), 1837-1845 (2001).
50. J. B. Goodenough, A. Manthiram, A. C. W. P. James and P. Strobel, Lithium Insertion Compounds, Solid State Ionics (G. Nazri, R. A. Huggins and D. F. Shriver, Eds.), *Material Research Society Symposium Proceedings* 135, 391 (1989).
51. D. W. Murphy, R. J. Cava, S. M. Zahurak and A. Santoro, Ternary Li_xTiO_2 Phases From Insertion Reactions, *Solid State Ionics* 9-10(DEC), 413-417 (1983).
52. L. A. Depicciotto and M. M. Thackeray, Transformation Of Delithiated $LiVO_2$ To The Spinel Structure, *Materials Research Bulletin* 20(2), 187-195 (1985).
53. L. A. Depicciotto and M. M. Thackeray, Lithium Insertion Extraction Reactions With $LiVO_2$ And LiV_2O_4, *Solid State Ionics* 18-9, 773-777 (1986).
54. G. Pistoia, M. Pasquali, L. A. Depicciotto and M. M. Thackeray, Behavior Of The Spinel LiV_2O_4 As A Positive Electrode For Secondary Li Cells, *Solid State Ionics* 28, 879-885 (1988).
55. M. M. Thackeray, W. I. F. David, P. G. Bruce and J. B. Goodenough, Lithium Insertion Into Manganese Spinels, *Materials Research Bulletin* 18(4), 461-472 (1983).
56. M. H. Rossouw, A. Dekock, L. A. Depicciotto and M. M. Thackeray, Structural Aspects Of Lithium-Manganese-Oxide Electrodes For Rechargeable Lithium Batteries, *Materials Research Bulletin* 25(2), 173-182 (1990).
57. F. Lubin, A. Lecerf, M. Broussely and J. Labat, Chemical Lithium Extraction From Manganese Oxides For Lithium Rechargeable Batteries, *J. Power Sources* 34(2), 161-173 (1991).
58. K. M. Colbow, J. R. Dahn and R. R. Haering, Structure And Electrochemistry Of The Spinel Oxides $LiTi_2O_4$ And $Li_{4/3}Ti_{5/3}O_4$, *J. Power Sources* 26(3-4), 397-402 (1989).
59. L. A. Depicciotto and M. M. Thackeray, Lithium Insertion Into The Spinel $LiFe_5O_8$, *Materials Research Bulletin* 21(5), 583-592 (1986).
60. M. Wakihara and O. Yamanoto, *Lithium Ion Batteries*, (Wiley-VCH, New York, 1998).
61. K. A. Striebel, A. Rougier, C. R. Horne, R. P. Reade and E. J. Cairns, Electrochemical studies of substituted spinel thin films, *J. Electrochem. Soc.* 146(12), 4339-4347 (1999).
62. R. Srinivasan, B. Braren, D. E. Seeger and R. W. Dreyfus, Photochemical Cleavage Of A Polymeric Solid - Details Of The Ultraviolet-Laser Ablation Of Poly(Methyl Methacrylate) At 193-Nm And 248-Nm, *Macromolecules* 19(3), 916-921 (1986).

80. J. E. Andrew, P. E. Dyer, D. Forster and P. H. Key, Direct Etching Of Polymeric Materials Using A XeCl Laser, *Appl. Phys. Lett.* 43(8), 717-719 (1983).
81. R. Srinivasan and B. Braren, Ablative Photodecomposition Of Polymer-Films By Pulsed Far-Ultraviolet (193 Nm) Laser-Radiation - Dependence Of Etch Depth On Experimental Conditions, *J. Polym. Sci. Pol. Chem.* 22(10), 2601-2609 (1984).
82. M. Schumann, R. Sauerbrey and M. C. Smayling, Permanent Increase Of The Electrical-Conductivity Of Polymers Induced By Ultraviolet-Laser Radiation, *Appl. Phys. Lett.* 58(4), 428-430 (1991).
83. T. Feurer, R. Sauerbrey, M. C. Smayling and B. J. Story, Ultraviolet-Laser-Induced Permanent Electrical-Conductivity In Polyimide, *Appl. Phys. A-Mater. Sci. Process.* 56(3), 275-281 (1993).
84. Z. Ball, T. Feurer, D. L. Callahan and R. Sauerbrey, Thermal and mechanical coupling between successive pulses in KrF-excimer-laser ablation of polyimide, *Appl. Phys. A-Mater. Sci. Process.* 62(3), 203-211 (1996).
85. J. Wei, N. Hoogen, T. Lippert, O. Nuyken and A. Wokaun, Novel laser ablation resists for excimer laser ablation lithography. Influence of photochemical properties on ablation, *J. Phys. Chem. B* 105(6), 1267-1275 (2001).
86. T. Lippert, J. Wei, A. Wokaun, N. Hoogen and O. Nuyken, Polymers designed for laser microstructuring, *Appl. Surf. Sci.* 168(1-4), 270-272 (2000).
87. T. Lippert, J. Wei, A. Wokaun, N. Hoogen and O. Nuyken, Development and structuring of combined positive-negative/negative-positive resists using laser ablation as positive dry etching technique, *Macromol. Mater. Eng.* 283(10), 140-143 (2000).
88. J. Wei, N. Hoogen, T. Lippert, C. Hahn, O. Nuyken and A. Wokaun, Characterisation of combined positive-negative photoresists by excimer laser ablation, *Appl. Phys. A-Mater. Sci. Process.* 69, S849-S853 (1999).
89. T. Lippert, C. David, J. T. Dickinson, M. Hauer, U. Kogelschatz, S. C. Langford, O. Nuyken, C. Phipps, J. Robert and A. Wokaun, Structure property relations of photoreactive polymers designed for laser ablation, *J. Photochem. Photobiol. A-Chem.* 145(3), 145-157 (2001).
90. T. Lippert, L. S. Bennett, T. Nakamura, H. Niino and A. Yabe, Single pulse threshold and transmission behaviour of a triazeno-polymer during pulsed UV-laser irradiation, *Appl. Surf. Sci.* 96-8, 601-604 (1996).
91. H. Fukumura, E. Takahashi and H. Masuhara, Time-Resolved Spectroscopic And Photographic Studies On Laser-Ablation Of Poly(Methyl Methacrylate) Film Doped With Biphenyl, *J. Phys. Chem.* 99(2), 750-757 (1995).
92. R. Srinivasan, K. G. Casey, B. Braren and M. Yeh, The Significance Of A Fluence Threshold For Ultraviolet-Laser Ablation And Etching Of Polymers, *J. Appl. Phys.* 67(3), 1604-1606 (1990).
93. H. Furutani, H. Fukumura and H. Masuhara, Photothermal transient expansion and contraction dynamics of polymer films by nanosecond interferometry, *J. Phys. Chem.* 100(17), 6871-6875 (1996).
94. H. Kim, J. C. Postlewaite, T. Zyung and D. D. Dlott, Ultrafast Imaging Of Optical-Damage Dynamics And Laser-Produced Wave-Propagation In Poly(Methyl Methacrylate), *J. Appl. Phys.* 64(6), 2955-2958 (1988).
95. M. Hauer, D. J. Funk, T. Lippert and A. Wokaun, Time resolved techniques as probes for the laser ablation process, *Optics and Laser Engineering* 43, 545 (2005).
96. H. Furutani, H. Fukumura and H. Masuhara, Nanosecond Time-Resolved Interferometric Study On Morphological Dynamics Of Doped Poly(Methyl Methacrylate) Film Upon Laser-Ablation, *Appl. Phys. Lett.* 65(26), 3413-3415 (1994).

114. M. J. Montenegro, C. Clerc, T. Lippert, S. Muller, P. R. Willmott, A. Weidenkaff and A. Wokaun, Analysis of the plasma produced by pulsed reactive crossed-beam laser ablation of $La_{0.6}Ca_{0.4}CoO_3$, *Appl. Surf. Sci.* 208, 45-51 (2003).
115. T. Scharf and H. U. Krebs, Influence of inert gas pressure on deposition rate during pulsed laser deposition, *Appl. Phys. A-Mater. Sci. Process.* 75(5), 551-554 (2002).
116. J. A. Bard and L. R. Faulkner, *Electrochemical Methods*, (John Wiley & Sons, New York, 2000).
117. M. Morcrette, P. Barboux, J. Perriere and T. Brousse, $LiMn_2O_4$ thin films for lithium ion sensors, *Solid State Ionics* 112(3-4), 249-254 (1998).
118. A. Rougier, K. A. Striebel, S. J. Wen and E. J. Cairns, Cyclic voltammetry of pulsed laser deposited $Li_xMn_2O_4$ thin films, *J. Electrochem. Soc.* 145(9), 2975-2980 (1998).
119. A. Rougier, K. A. Striebel, S. J. Wen, T. J. Richardson, R. P. Reade and E. J. Cairns, Characterization of pulsed laser-deposited $LiMn_2O_4$ thin films for rechargeable lithium batteries, *Appl. Surf. Sci.* 134(1-4), 107-115 (1998).
120. C. Julien, E. Haro-Poniatowski, M. A. Camacho-Lopez, L. Escobar-Alarcon and J. Jimenez-Jarquin, Growth of $LiMn_2O_4$ thin films by pulsed-laser deposition and their electrochemical properties in lithium microbatteries, *Mater. Sci. Eng. B-Solid State Mater. Adv. Technol.* 72(1), 36-46 (2000).
121. D. Singh, W. S. Kim, V. Craciun, H. Hofmann and R. K. Singh, Microstructural and electrochemical properties of lithium manganese oxide thin films grown by pulsed laser deposition, *Appl. Surf. Sci.* 197, 516-521 (2002).
122. D. Singh, *Influence of microstructure on electrochemical properties of Li-Mn-O thin films*, Thesis at Ecole Polytechnique Fédéral de Lausanne (2001).
123. M. Morcrette, P. Barboux, J. Perriere, T. Brousse, A. Traverse and J. P. Boilot, Non-stoichiometry in $LiMn_2O_4$ thin films by laser ablation, *Solid State Ionics* 138(3-4), 213-219 (2001).
124. M. Inaba, T. Doi, Y. Iriyama, T. Abe and Z. Ogumi, Electrochemical STM observation of $LiMn_2O_4$ thin films prepared by pulsed laser deposition, *J. Power Sources* 81, 554-557 (1999).
125. C. M. Julien and M. Massot, Lattice vibrations of materials for lithium rechargeable batteries III. Lithium manganese oxides, *Mater. Sci. Eng. B-Solid State Mater. Adv. Technol.* 100(1), 69-78 (2003).
126. T. Dumont, T. Lippert, M. Döbeli, H. Grimmer, J. Ufheil, P. Novák, A. Würsig, U. Vogt and A. Wokaun, Influence of experimental parameter on the Li-content of $LiMn_2O_4$ electrodes produced by pulsed laser deposition, *Appl. Surf. Sci.* article in press, (2006).